THE PLANT CELL

The Plant Cell, 2025, **37**, koaf143

https://doi.org/10.1093/plcell/koaf143
Advance access publication 23 July 2025
Review

Best practices in plant fluorescence imaging and reporting: A primer

Kirk J. Czymmek,[1,*] Yoselin Benitez-Alfonso,[2] Tessa Burch-Smith,[3] Luigi F. Di Costanzo,[4] Georgia Drakakaki,[5] Michelle Facette,[6] Daniel Kierzkowski,[7] Anastasiya Klebanovych,[1] Ivan Radin,[8] Suruchi Roychoudhry,[2] Heather E. McFarlane[9,*]

[1]Advanced Bioimaging Laboratory, Donald Danforth Plant Science Center, St. Louis, MO 63132, USA
[2]Centre for Plant Sciences, School of Biology, University of Leeds, Leeds LS2 9JT, UK
[3]Donald Danforth Plant Science Center, St. Louis, MO 63132, USA
[4]Department of Agricultural Sciences, University of Naples Federico II, Portici 80055, Italy
[5]Department of Plant Sciences, University of California Davis, Davis, CA 95616, USA
[6]Department of Biology, University of Massachusetts, Amherst, MA 01003, USA
[7]Département de Sciences Biologiques, Institut de Recherche en Biologie Végétale, Université de Montréal, Montréal, QC H1X 2B2, Canada
[8]Department of Plant and Microbial Biology, University of Minnesota, Saint Paul, MN 55108, USA
[9]Department of Cell and Systems Biology, University of Toronto, Toronto, ON M5S 3B2, Canada
*Author for correspondence: kczymmek@danforthcenter.org (K.J.C.), h.mcfarlane@utoronto.ca (H.E.M.)
The author(s) responsible for distribution of materials integral to the findings presented in this article in accordance with the policy described in the Instructions for Authors (www.plantcell.org) is (are): Kirk J Czymmek (kczymmek@danforthcenter.org).

Abstract

Microscopy is a fundamental approach for plant cell and developmental biology as well as an essential tool for mechanistic studies in plant research. However, setting up a new microscopy-based experiment can be challenging, especially for beginner users, when implementing new imaging workflows or when working in an imaging facility where staff may not have extensive experience with plant samples. The basic principles of optics, chemistry, imaging, and data handling are shared among all cell types. However, unique challenges are faced when imaging plant specimens due to their waxy cuticles, strong/broad spectrum autofluorescence, recalcitrant cell walls, and air spaces that impede fixation or live imaging, impacting sample preparation and image quality. As expert plant microscopists, we share our collective experience on best practices to improve the quality of published microscopy results and promote transparency, reproducibility, and data reuse for meta-analyses. We offer plant-specific advice and examples for microscope users at all stages of fluorescence microscopy workflows, from experimental design through sample preparation, image acquisition, processing, and analyses, to image display and methods reporting in manuscripts. We also present standards for methods reporting that will be valuable to all users and offer tools to improve reproducibility and data sharing.

Introduction

Imaging experiments can provide invaluable mechanistic and quantifiable insights into biological processes, and they have become essential for modern plant biology studies. Light microscopy is arguably the most widely used imaging approach in plants (Gilroy 1997; Berg and Beachy 2008; Ovečka et al. 2018; Colin et al. 2022). While other imaging approaches such as electron microscopy (Wilson and Bacic 2012; Engel et al. 2015; Otegui and Pennington 2019; Wightman 2022; Wickramanayake and Czymmek 2023), X-ray microscopy (Piovesan et al. 2021; Duncan et al. 2022), atomic force microscopy (Kirby et al. 1996), MS imaging (Zou et al. 2025), and high-throughput phenotyping (Fahlgren-Gehan, and Baxter 2015) have been applied to plant research, light microscopy dominates the literature in plant biology as an accessible, convenient, efficient, and powerful approach to address important scientific questions in plant research. Fluorescence microscopy, in particular, can be used to localize fluorescently tagged proteins of interest in cells or tissues. The localization of cellular components, such as nucleic acids (Tirichine et al. 2009), polysaccharides (Piccinini et al. 2024), lipids (Chu et al. 2022), hormones (Balcerowicz et al. 2021; Herud-Sikimić et al. 2021), ions, or other metabolites (Monshausen et al. 2008) within cells or tissues are readily possible. In addition, fluorescent probes can be used to track developmental processes and cellular growth, compare wild type with mutant or genetically engineered plants, and/or compare control with plants treated with external agents. Samples can be viewed live or fixed during microscopy experiments, depending on the biological question at hand. Often, components of interest (organelles, proteins, metabolites, etc.) will be tagged with fluorescent molecules such as fluorescent protein fusions in live or fixed cells (Haseloff 1999; Berg and Beachy 2008; Wu et al. 2013), including the convenient use of transient expression in tobacco leaves or protoplasts, localized via immunolabeling of fixed cells (Baskin et al. 1992; Lee and Knox 2014; Shimamura 2015), or identified using fluorescent stains (Hepler and Gunning 1998; Yu et al. 2008; Shaw and Ehrhardt 2013), all of which are widely used in plant biology. More sophisticated imaging approaches, such as fluorescence recovery after photobleaching (Scheuring et al. 2024), Förster resonance

Received April 05, 2025. Accepted May 19, 2025.

energy transfer (Krebs et al. 2012), fluorescence correlation spectroscopy (Clark et al. 2016), fluorescence lifetime imaging microscopy (Noble et al. 2017), bimolecular fluorescence complementation (Waadt and Kudla 2008), multiphoton microscopy (Kurihara et al. 2015; Mizuta 2021), variable angle total internal reflection fluorescence microscopy (Wan et al. 2011), and expansion microscopy (Kao and Nodine 2021; Cox et al. 2025) can be used to understand molecular interactions and their dynamics, but these techniques are outside the scope of this review, which is intended as a primer for novice and intermediate fluorescence microscope users.

Imaging experiments and analyses must be rigorously designed, and results must be judiciously interpreted and carefully communicated to ensure that the underlying data generated support the authors' claims. Indeed, there are numerous considerations and pitfalls that must be accounted for to achieve reliable, reproducible, and meaningful results when using fluorescence imaging. Best practices in fluorescence imaging have been emphasized in several excellent overviews elsewhere (Lichtman and Conchello 2005; North 2006; Montero Llopis et al. 2021), and while many of the same guiding principles apply to plants, these use cases are typically focused on biomedical imaging using cell culture or animal tissue examples. Here, we provide practical guidelines focused on the fundamentals of fluorescence imaging and solutions for specific and unique challenges that plant biologists often face. These guidelines are aimed at beginning or intermediate microscopists but also offer standards that even advanced users could find useful. Like any scientific pursuit, excellence in imaging is an iterative process that is always grounded in the biological question being asked. We walk users through the steps of fluorescence imaging experiments from initial experimental setup, experimental design, sample preparation, image acquisition, through to data processing and analysis, image display and finally, methods reporting in manuscripts using plant-specific examples (Fig. 1). Importantly, before undertaking a large-scale imaging experiment we suggest a smaller pilot project with an expert mentor following the proposed imaging workflow (Fig. 1). Establishing a "design, test, learn, and iterate" mindset, creates a rapid feedback loop to address any unanticipated challenges and to make any refinements, accordingly. Our collective experience as instructors and microscopists has led us to emphasize the common insights, misconceptions, and pitfalls that newer users may experience. Ultimately, the goal of this manuscript is to help shorten the learning curve, improve experimental quality, foster reproducibility, and support success when fluorescence microscopy is applied to plant research.

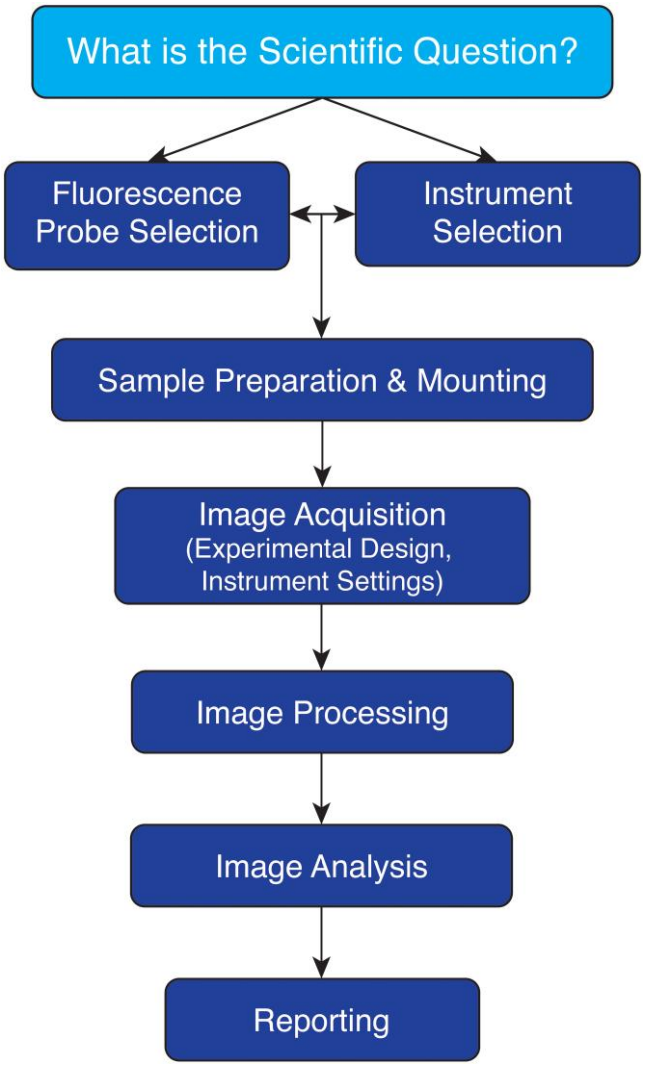

Figure 1. Key steps to imaging experiment workflow. **1)** Consider fluorescence probe and instrument selection, which are often interdependent and based on resource availability. **2)** Select appropriate sample preparation and mounting conditions. **3)** Image acquisition includes appropriate experimental design (e.g. controls) and instrument settings to obtain meaningful qualitative and/or quantitative results. Multiple imaging modalities and platforms may be useful to answer different aspects of a scientific question, and the experiment setup may need to be refined depending on preliminary results. **4)** Image processing (if necessary) with documentation may be performed to facilitate visualization and/or quantification of target features, while **5)** Image analysis will translate image data into measurable quantitative comparisons of results. **6)** Reporting includes disclosure of any essential parameters to document these steps for reproducibility, peer review, and reader interpretation. Note that this workflow is meant to provide a useful and logical framework but sometimes workflow order may not necessarily be as linear or rigid as portrayed, especially when troubleshooting.

Instrument and fluorescence probe selection

Two of the most important upfront decisions when starting a plant imaging experiment are what probes to use and what type of microscope is best suited to answer the biological question. These two decisions are intrinsically linked. Ideally, one must consider the strengths and weaknesses of a particular imaging platform, including assessment of the experimental requirements for lateral (x–y) and axial (z) resolution, acquisition speed, sensitivity (high signal collection efficiency), and spectral (wavelength) separation, in a concept referred to as "Dimensions of Imaging" (Fig. 2). While this chart represents common imaging modalities and their representative strengths/limitations, a majority of biological questions can be answered on any of these platforms, albeit with some technology-related constraints (reviewed by Ovečka et al. 2018; Davidson et al. 2024). Practically speaking, many conventional widefield epi-fluorescence and/or confocal microscopes are suitable for many routine experiments.

Choosing an imaging platform

Widefield microscopes, which simultaneously illuminate the whole sample with a light source and collect emitted light, are likely to be the most accessible, flexible, affordable, and easy-to-use option for plant scientists (Fig. 3). Although widefield epi-fluorescence microscopy is generally only suitable for thinner samples, deconvolution algorithms can partially restore resolution, contrast, and signal using corrections derived from expected (theoretical) or measured (empirical) microscope performance

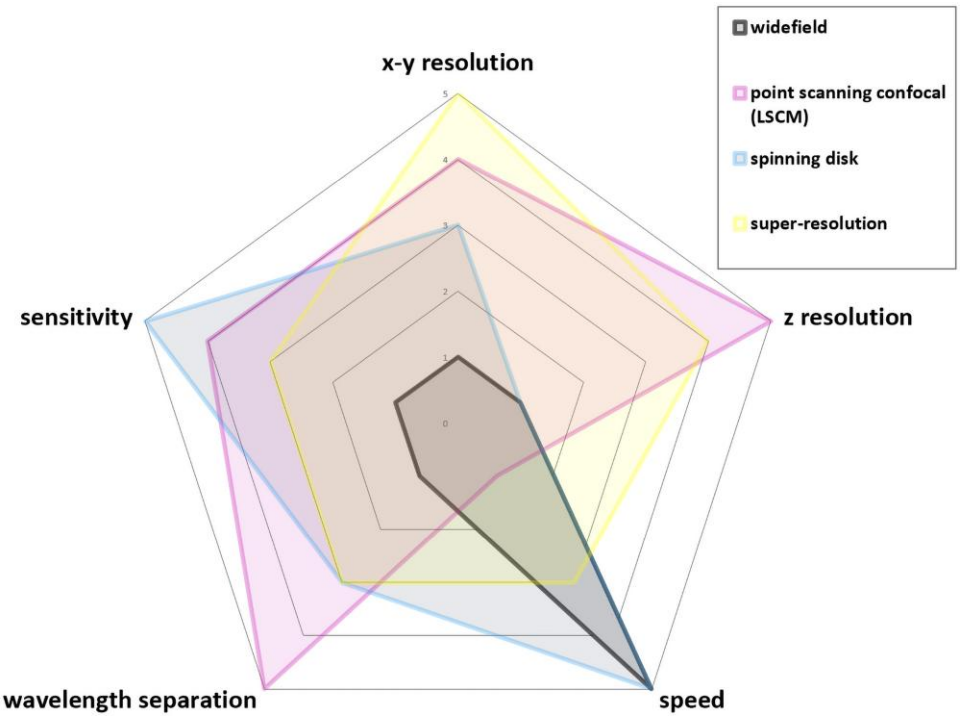

Figure 2. Dimensions of fluorescent imaging (and trade-offs). Selection of the optimal imaging platform depends on experimental goals. Super-resolution microscopy followed by point scanning confocal microscopy (aka LSCM) provide the greatest lateral (x–y) resolution, while spinning disk and widefield microscopy have the best speed for capturing dynamic events. Other criteria of note are the high signal collection efficiency (sensitivity) of spinning disk and the best z-resolution and wavelength separation with LSCM systems. Wavelength separation is best with spectral detection (more common in point scanning confocal microscopes) vs filter-based systems typically used in widefield and spinning disk systems. All platforms can be used for many plant imaging experiments, but some will perform better than others for certain tasks where resolution, dynamics, and/or spectral separation are critical. Note that this is a generalized chart and the exact proportional difference in each dimension is dependent upon the microscope setup and specific technique employed.

(McNally et al. 1999; Swedlow 2007; Wernersson et al. 2024). For example, the out-of-focus blur observed using widefield microscopy of a thick plant leaf (Fig. 3A) can be improved using deconvolution. The convenience and benefit of widefield microscopes should not be underestimated for many projects, especially for efficiently screening and documenting large sample sets, detecting weak signals (with high-end systems), and/or working with thin or thinly sectioned materials.

Laser scanning confocal microscopy (LSCM; also called point scanning confocal microscopy) is another primary workhorse for plant imaging experiments. LSCM excites fluorescent molecules using a laser focused to a point that is raster-scanned across the sample, and a pinhole aperture is used to reject out-of-focus emission light creating thin, high contrast "optical sections" (Fig. 3, B and C). When 2D optical sectioning is combined with motorized focus control, z-stacks can be generated and reconstructed into 3D perspectives (Fig. 3: compare Widefield 3D, Confocal 3D and Super-Resolution 3D). A drawback of LSCM is speed (Fig. 2), since it takes time to raster the laser point-by-point across the sample. However, technology such as detector element arrays (e.g. Zeiss Airyscan) can further improve scan speed and resolution of LSCM (Fig. 3G) (Scipioni et al. 2018; Kana et al. 2023).

When higher imaging speeds are required for cell dynamics studies (e.g. calcium imaging, cytoskeleton dynamics, vesicle trafficking, or fast 3D collection; (Ueda et al. 2010; Oreopoulos et al. 2014; Verbančič et al. 2021) spinning disk confocal microscopy (Fig. 3, E and F) with multiple pinhole optics is often the tool of choice. Spinning disk confocal microscopy can capture data at imaging rates of ~100+ frames/s. Practically speaking, imaging rates will be much slower for many experiments. Fast imaging on spinning disk systems reduce photobleaching, relative to LSCM systems. Like LSCM, spinning disc systems can effectively be combined with the benefits of deconvolution (compare Fig. 3, E and F).

Super-resolution microscopy (Sydor et al. 2015; Hickey et al. 2021) is appropriate when resolution is paramount to visualize features 2 to 10× below the diffraction limit (~250 nm with green light) such as with sub-organellar studies (e.g. localization of nuclear structures and pores [Schubert 2017], plasmodesmata [Bell et al. 2013; Czymmek et al. 2023], and others as reviewed in Komis et al. [2015] and Ovečka et al. [2022]). A few common super-resolution techniques include single molecule localization microscopy approaches, such as photoactivated localization microscopy and stochastic optical reconstruction microscopy, structured illumination microscopy, and stimulated emission depletion microscopy. With these more advanced techniques (Leung and Chou 2011), we strongly encourage consultation with an expert to assess feasibility and benefits/limitations for individual research goals.

Another factor to consider is whether the best microscope to use is upright (the objective lens above the sample) or inverted (the objective lens below the sample) or vertical (the objective lens and sample both horizontal). In general, upright and inverted configurations are readily amenable to traditional slide-mounted specimens, although dipping lenses (that can directly contact the specimen medium) are primarily used with upright configurations (see Tips for working with live samples). Inverted microscopes can work well with certain live experiments where extra space or access above the objective lens is required, such as for a heating stage, manipulators, or multi-well plates.

System performance is a function of the entire system's light path, including characteristics of all optical elements

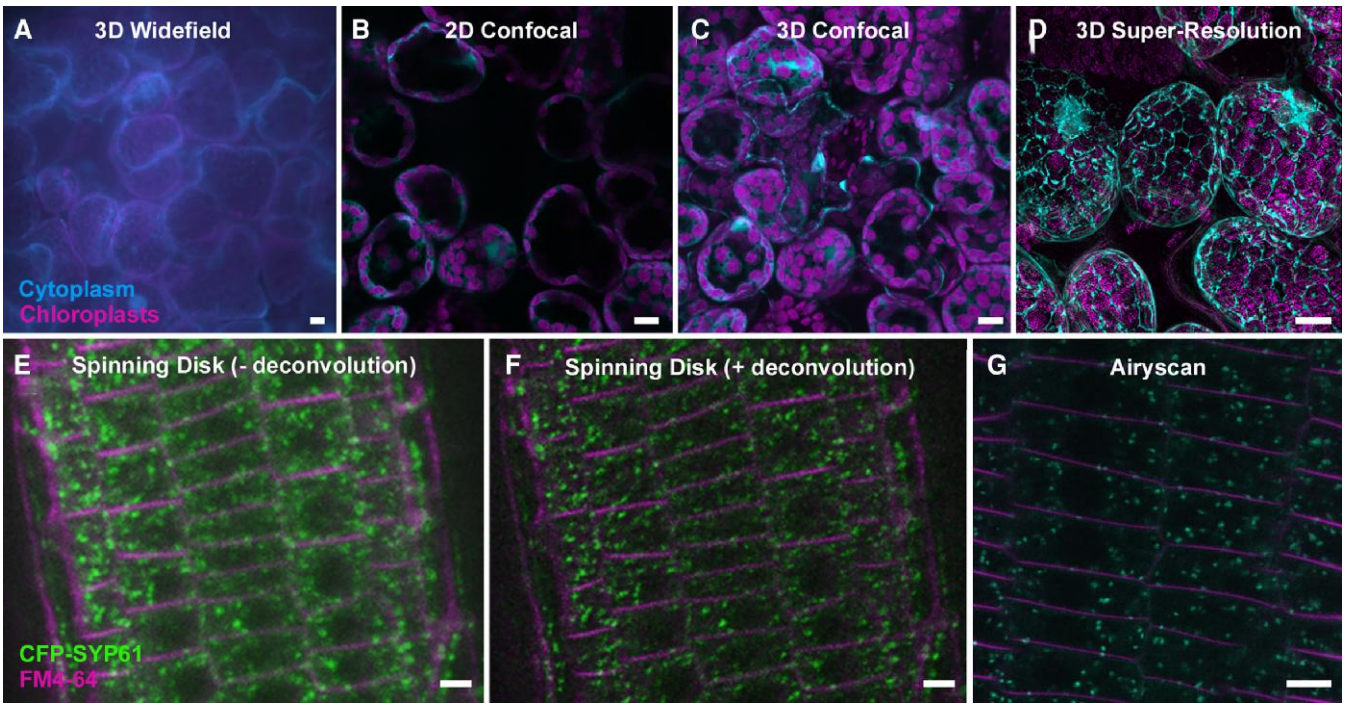

Figure 3. Plant leaf and root imaging comparing common fluorescence imaging modes. **A-D)** A comparison of image contrast and detail with cytoplasmic expression of untagged CFP and chloroplast chlorophyll autofluorescence in *N. benthamiana* leaf mesophyll cells. **A)** 3D Widefield microscopy (z-stack maximum intensity projection) exhibited the lowest contrast while a single 2D optical section **(B)** and 3D confocal z-stack maximum intensity projection **(C)** showed increased contrast and cellular detail, while **(D)** 3D super-resolution (z-stack maximum intensity projection) provided the greatest cellular detail (resolution). **E-G)** *A. thaliana* root division zone cell imaging of membrane stain, FM4-64 and Syntaxin of Plants 61 CFP-SYP61 comparing signal-to-noise, contrast and cellular detail from 3i spinning disk without **(E)** and with **(F)** deconvolution to ZEISS LSM980 Airyscan imaging **(G)**; full details of the microscope hardware, software, and imaging setup for this and all other figures are supplied in Supplementary Table S1. Scale bars A-D = 10 μm, E-G = 5 μm.

(filters, mirrors, objective lens, etc.) and the detector (a camera array vs point detector photo-multiplier tube [PMT]). For example, considering just the detector, high-sensitivity scientific complementary metal oxide semiconductor cameras can detect up to 95% of photons that reach it (referred to as its quantum efficiency) compared with ~45% for gallium arsenide phosphide photocathode (PMT) or 20% for traditional PMTs; these differences in sensitivities are also wavelength dependent (Montero Llopis et al. 2021). Ultimately, if weaker signals are anticipated, a more sensitive configuration may be critical.

Selecting fluorescent probes

Once the imaging approach is selected, it is important to determine what light sources/wavelengths and filters are available and to match these with the appropriate fluorescent probe. Here, widefield epi-fluorescence microscopy typically has some flexibility by using low-cost and broad-spectrum white light (e.g. mercury or xenon arc lamps, metal halide lamps) or light emitting diodes as light sources (Aswani et al. 2012). Most epi-fluorescence systems use filter cubes (containing filters and a dichroic mirror (specialized optical elements that differentially reflect/transmit light) to separate the excitation/emission light path (Supplementary Fig. S1) matched to the corresponding wavelengths appropriate for imaging the selected fluorescence probe(s). While the majority of systems will have common filter sets for blue (e.g. UV dyes, DAPI, calcofluor white), green (e.g. GFP, fluorescein isothiocyanate [FITC], AlexaFluor 488), and red (e.g. RFP, mCherry, rhodamine, Texas red, AlexaFluor 546, propidium iodide) fluorophores, other fluorophores (e.g. CFP, YFP) or longer wavelength fluorophores (e.g. chlorophyll A/B autofluorescence, Cy5 and AlexaFluor 660, or near-infrared probes) may require additional appropriate filters. Furthermore, filter sets can be long pass (having a wide emission range, e.g. 500 nm and all wavelengths above) or band pass (having a narrow emission range, e.g. 500 to 550 nm), and this distinction can have important implications for the experiment. For example, when working with leaf tissue, chlorophyll autofluorescence (650 to 700 nm) will often contribute undesirable signal (bleed-through or crosstalk) to the emission spectra of most lower wavelength fluorophores in the absence of band pass filters. Likewise, multiple fluorophore imaging almost always requires band pass filters to separate different fluorophores.

Many laser-based imaging systems, such as LSCM or spinning disk microscopes, have discrete high-powered laser lines (e.g. 405, 488, 514, 561, and 640 nm) or broader spectrum and/or tunable excitation ranges (e.g. white light or multi-photon lasers). Dichroic mirrors, filters, prisms, and/or diffraction gratings separate the excitation and emission pathways (Fig. 4) in laser-based systems. Notably, prisms or diffraction gratings in the emission pathway can be combined with sliders that are user definable, which allows flexible wavelength ranges and spectral imaging of fluorophore emission signals. Spectral imaging, in which a series of images collected at continuous discrete wavelength bands (e.g. 10 nm windows) along a defined spectrum (e.g. 400 to 600 nm), can be used to generate emission fingerprints and processed via linear unmixing to separate closely overlapping fluorophores. This capability is especially useful to help remove (unmix) various forms of plant autofluorescence that may contaminate target signals and/or to separate closely overlapping

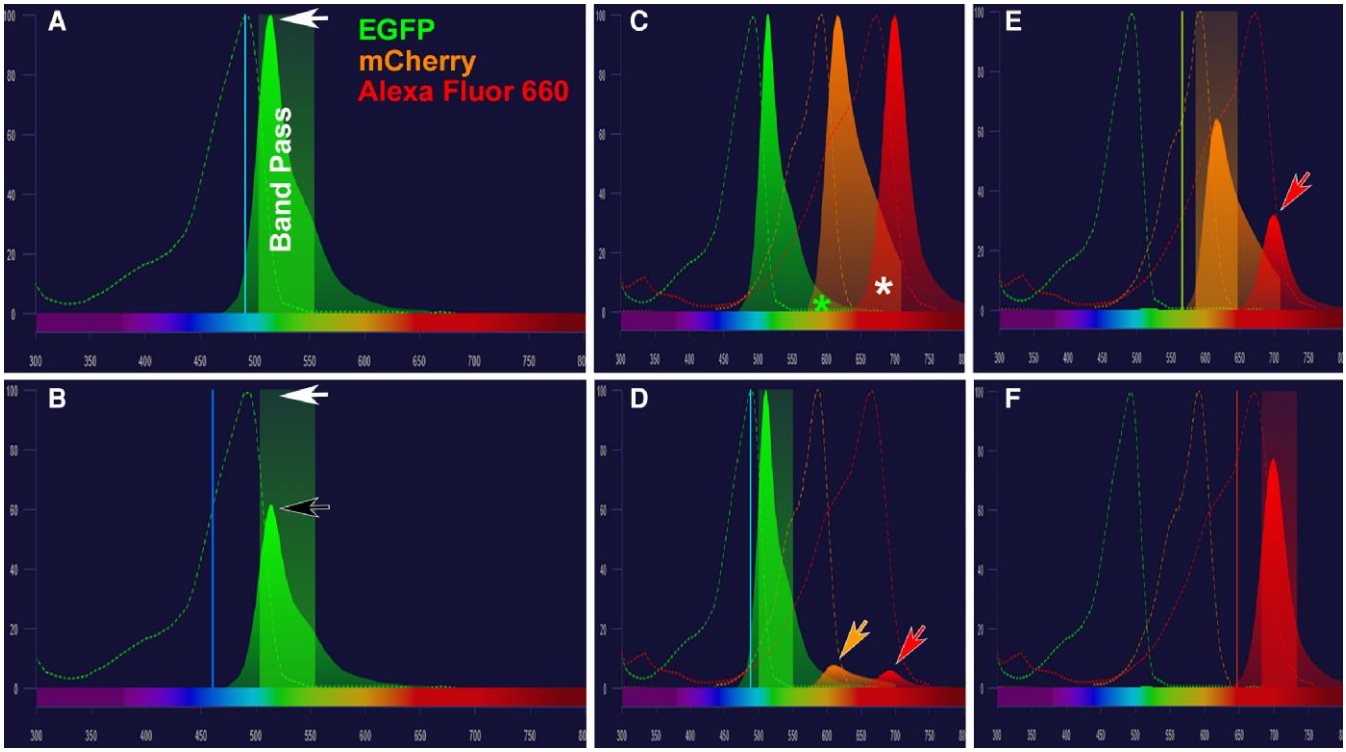

Figure 4. Fundamentals of excitation (dashed lines, unfilled curves) and emission spectra (solid lines, filled curves) and their relationship to microscope excitation (single vertical lines) and emission filters (thick vertical bars). **A)** The fluorescence emission maximum from EGFP (white arrow) when excited with 488-nm laser (vertical cyan line) and collected with 525/50 (500 to 550 nm) bandpass emission filter (transparent green thick vertical bar). **B)** With suboptimal 458-nm excitation of EGFP (compare white vs black arrow), there is an ~40% decrease in peak emission intensity compared with 488-nm laser excitation when using the same emission filter as **(A)**. **C)** When performing multicolor experiments, fluorophore selection (including potential autofluorescence) and imaging setup/strategy must be carefully considered to avoid detection of emission signal overlap due to crosstalk. Note emission spectra overlap portions (white asterisks) of the EGFP, mCherry and Alexa Fluor 660 signals. **D)** Imaging of 1 dye at a time with EGFP (488-nm excitation, 525/50 bandpass emission filter) still excites and collects mCherry (arrow) and Alexa Fluor 660 (arrow) signals, but this sequential imaging limits crosstalk into the EGFP image. **E)** Likewise, sequential imaging of mCherry (561-nm excitation, 610/60 bandpass emission filter) prevents excitation shorter wavelength fluorophores (i.e. EGFP) and reduces Alexa Fluor 660 (arrow) crosstalk in the mCherry image. **F)** Finally, sequential imaging of Alexa Fluor 660 (640-nm excitation, 700/50 bandpass emission filter) prevents any lower wavelength fluorophore crosstalk into the image. Spectra created using ThermoScientific Fluorescence SpectraViewer (Thermofisher 2024).

fluorophores (Hardham 2012; Conéjéro et al. 2014) to allow more fluorescent probes to be used in an experiment (Zimmermann et al. 2014). See Controls on strategies to ensure that crosstalk does not impact multi-color experiments.

Ultimately, the microscope's excitation and emission configuration and the fluorescent probes need to be carefully matched. However, there is some forgiveness with filter sets and fluorophore choice, allowing sufficient excitation and emission signals to be collected even if not perfectly matched (e.g. a GFP filter set can be used to image YFP in many cases). Nevertheless, when fluorophore choice is flexible in experimental design and/or target molecule(s) are of low abundance and optimized conditions are critical, it is prudent to determine system light sources and excitation/emission configuration and to refer to excellent publicly available tools for optimizing probe choices with system configuration (Fig. 4). See FPbase.org (Lambert 2019) for fluorescent proteins, (Thermofisher 2024) for common organic dyes, and (Stewart 2001; Malabadi et al. 2008; Colin et al. 2022) for plant-specific genetically encoded probes.

When constructing genetically encoded fluorescent protein fusions, there are important considerations beyond fluorophore selection, including promoter selection and fluorescent protein fusion orientation. For example, the choice of promoter, fluorescent protein, and fusion orientation can all have profound effects on the behavior of actin binding fluorescent probes for visualizing the plant cytoskeleton (Wang et al. 2008; Dyachok et al. 2014). Additionally, consider using a monomeric version when working with fluorescent protein fusions. Multimerization of fluorescent proteins is very common and while it can improve brightness, it can cause aggregation, affecting the localization pattern and/or function of target proteins (Campbell et al. 2002 ; Segami et al. 2014). Ideally, new fluorescent protein fusions are tested for functionality by the ability of the fusion protein to complement knockout mutant phenotypes before conducting imaging experiments.

Simply matching a fluorophore and system configuration is not always sufficient. The properties of a fluorophore also can play a role in imaging success, such as its pH/environmental sensitivity, size, photostability (resistance to bleaching) (Shaner et al. 2013; Tanz et al. 2013; Voss et al. 2013; Duwé and Dedecker 2019; Colin et al. 2022), and its overall brightness. Brighter probes allow for more gentle imaging (lower excitation power), improved signal-to-noise, and faster acquisition times, which are all particularly important for live-cell imaging. The relative brightness of a probe can be calculated as the extinction coefficient (EC—likelihood of a fluorophore absorbing excitation light) multiplied by the quantum yield (QY—the fraction of absorbed photons that result in fluorescence emission) divided by 1,000 (McNamara 2024). For example, enhanced GFP (EGFP) (EC = 55,900, QY = 0.6) has a relative brightness of 33.54, while mNeonGreen (EC = 116,000, QY = 0.8) has a relative brightness of 92.8 and is nearly 3× brighter.

Although not all fluorophores are equal, many probes can be used interchangeably without issues. When flexibility is possible (e.g. starting experimental design from scratch) and/or the biological question demands specific conditions (low expression levels, high-speed imaging of dynamic events, multi-fluorophore imaging, autofluorescence challenges, etc.), optimizing probe choice for the biological question and the imaging system will increase the chances of a successful outcome and allow far greater versatility in imaging approaches across the dimensions of fluorescence imaging (Fig. 2).

Sample preparation and mounting

A critical step of successful plant imaging is sample preparation. There are at least 4 very important questions that should be part of that decision-making process: (1) Will the sample be live or fixed? (2) What microscope/objective lens is required to achieve the imaging goals? (3) How will the sample be mounted to ensure adequate optical quality? and (4) What controls are required to ensure that image features are not a result of optical, fixation, or other preparation-induced artifacts?

Tips for working with live samples

Imaging living samples is usually convenient and fast (preparation steps are generally less involved) and since samples are not fixed, fixation artifacts can be avoided, and dynamic events can be recorded. However, living samples are typically removed from their experimental growth conditions/environment and/or excised before mounting, which can cause substantial changes to the sample, including wounding responses and cell death. Indeed, some dyes tend to stain tissue more quickly at or adjacent to damaged or cut regions, leading to the temptation to image these sites (Truernit and Haseloff 2008). Users should avoid imaging areas of cell damage or death (unless scoring viability), since these images will not be biologically relevant and will not reflect the reality of healthy, living cells (see Controls for live-cell imaging below).When working with aerial tissues, such as leaves, stems, or flowers, bubbles of air may be trapped between the epidermis and coverslip due to the hydrophobic waxy cuticle. These are relatively straightforward to identify as transmitted light images readily reveal the air bubble edge, and the sample itself tends to have higher contrast in those areas. Avoid imaging within these regions as light scattering will severely impact optical quality and affect qualitative and quantitative results. Surface air bubbles can be reduced by adding surfactants such as 0.01% Silwet or Tween-20 (Zhao et al. 2017; Huynh et al. 2022) in aqueous sample mounting media. Intracellular air spaces can be infiltrated using gentle vacuum/syringe pressure to replace the air spaces in the spongy mesophyll with an aqueous medium to improve dye staining and optical continuity (Supplementary Fig. S2). When working with tissues that lack a waxy cuticle, particular care must be taken during sample preparation and mounting to avoid drying the tissue (Sawchuk et al. 2007; Prunet et al. 2016; Ovečka et al. 2018; Zhu et al. 2020; Silveira et al. 2022). For deep or long-term imaging, nontoxic and non–cell-permeable media with low surface tension and excellent optical and gas exchange properties may be useful, such as Perfluorodecalin (a component of artificial blood) and its derivatives (Littlejohn et al. 2010, 2014). Long-term imaging under the coverslip may lead to the compression of observed samples; this can influence the organization of structures such as the microtubule cytoskeleton, which is mechanoresponsive (Hamant et al. 2008; Jacques et al. 2013). These effects can be partially mitigated by using adequate spacers between mounting slides and coverslips that prevent mechanical compression of the tissue and by reducing water evaporation during imaging. For many developmental studies, a more specialized lightsheet (Ovečka et al. 2018) or upright microscope configuration with dipping lenses are often the best choice, if available (Zhu et al. 2020; Silveira et al. 2022). When using dipping lenses, samples are often mounted on agar medium in small Petri dishes or other plastic containers. The presence of air bubbles on the surface of the sample and sample movement can pose problems when imaging with dipping objectives, requiring additional preventive measures to avoid artifacts such as localized signal loss and geometric distortions of the sample (Sawchuk et al. 2007; Prunet et al. 2016).

Tips for working with fixed samples

For fixed samples, a broad range of affinity probes are available, such as stains, antibodies, or in situ hybridization to detect nucleic acids. Additionally, with appropriate fixation protocols, fluorescent protein signals can be retained (Nybo 2012; Kurihara et al. 2015). Samples can be fixed, typically in aldehydes, and imaged intact as a whole mount (Truernit et al. 2008; Kurihara et al. 2015) or prepared for sectioning via hand sections, vibratome (Leroux 2020), cryostat (Tirichine et al. 2009; Knapp et al. 2012), or microtomy (Baskin et al. 1992; Marion et al. 2017). Which sectioning approach is most appropriate will depend on tissue type and size, desired section thickness, probe accessibility needs, and the capabilities of the selected imaging platform. Generally, hand sections will be thicker (millimeter scale) and more variable, vibratome and cryostats can reliably produce sections (tens of microns), while microtomy of resin-embedded specimens can yield sections ranging from tens of nanometers to a few microns. To identify an appropriate sectioning strategy, we suggest identifying a publication with similar probe types and imaging goals and/or contacting a domain expert. Antibodies and other larger probes can be used to label sections, or with special treatment to disrupt or remove plant cell walls, such as enzyme or chemical permeabilization, or freeze shattering methods (Shimamura 2015; Celler et al. 2016), these large probes can be applied to whole-mount samples. Notably, the fixation strategy and buffers themselves can induce artifacts (Yoshida et al. 2023). When working with fixed specimen, autofluorescence can be a by-product of aldehyde fixation, especially glutaraldehyde. Use of 0.1% sodium borohydride (Clancy and Cauller 1998) can help reduce aldehyde induced autofluorescence, and addition of glycine can block unreacted aldehydes (Piña et al. 2022). In some instances, samples can be cleared (Kurihara et al. 2015; Hériché et al. 2022; Sakamoto et al. 2022) and/or mounting media with/without antifade components can be applied to improve the optical homogeneity throughout the sample for high quality, deeper imaging (Bassel and Smith 2016). Photobleaching results in chemical modification of a fluorophore (Mahmoudian et al. 2011), causing the irreversible loss of fluorescence. Antifade agents are chemical compounds that serve as oxygen free radical scavengers, which can reduce photobleaching. However, not all anti-fade agents are created equal, and many do not work effectively or universally for all probes and are toxic for living cells (Ono et al. 2001). For further reading to help select an appropriate mounting media, we recommend an excellent primer describing various mounting media components and comparing their performance (Collins 2006).

The objective lens, immersion medium, coverslip, and mounting medium

For high-resolution imaging of live or fixed samples, the sample mounting medium (the media in which the sample is suspended

in between the slide and the coverslip) should be considered as an extension of the objective lens. The mounting medium should be an optically and sample suitable solution (water, buffer, etc.) that considers both the sample and the objective lens.

Many objective lenses are labeled to use a specific immersion media (the media between the objective and the slide coverslip; e.g. air, water, oil) to achieve their designed performance specifications. With the exception of air lenses, a small droplet of immersion media is placed between the front lens element of the objective and the sample coverslip, ensuring optical continuity (no coverslip is used with a dipping lens—see Tips for working with live samples). For more detailed background reading, we highly recommend an excellent overview of the important characteristics and concepts of immersion media (Abramowitz and Davidson 2015).

Importantly, the NA of an objective lens has a dependency on the refractive index (RI) of the immersion medium (Keller 1990; Staudt and Hell 2008) and the more closely matched and uniform the RI of the objective immersion medium is to the sample and its mounting medium, the better the image quality (compare Fig. 5, A and B, air vs water infiltration). In simple terms, the objective lens numerical aperture (NA) essentially relates to the cone of light that is collected by the lens and represents its light gathering and x-y-z resolving power. For reference, common objective immersion media are as follows: air (RI = 1), water (RI = 1.33), glycerol (RI = 1.47), silicone (RI = 1.4), or oil (RI = 1.51). For example, this is illustrated by imaging a uniform 3% agarose gel (RI ~1.33, like many biological tissues) infiltrated with 1 μg/mL of FITC, demonstrating the effect of the objective lens on signal intensity from the coverslip to ~300 μm deep (Supplementary Fig. S3). In this homogeneous sample, there is a notable decrease in signal when using the 20× air lens (NA 0.7) and excellent uniformity with the 40× water lens (NA 1.2). Although there is substantial signal attenuation with the highest NA 100× lens (NA 1.4), the 100× lens outperforms these other lenses in resolution when imaging very near the coverslip (Supplementary Fig. S4). This example demonstrates the tradeoff between high resolution imaging with a low depth of imaging (e.g. with the high NA, 100× oil objective) and low-resolution imaging with a greater depth of imaging (e.g. with lower NA, 40× water objective). Additionally, even in this relatively uniform sample (Supplementary Fig. S3) and in more complex plant samples (Fig. 5), image quality and resolution are degraded due to spherical aberrations (Goodwin 2007; Diel et al. 2020) that increase in severity at increasing distances from the coverslip due to RI mismatch. This means the image quality, resolution and signal intensity can degrade rapidly away from the coverslip, compounded by many light-scattering plant structures. Even slide-to-slide variations in mounting medium thickness covering the sample can make a measurable difference in fluorescence signals and image quality. Nevertheless, in some instances, it is worthwhile to verify specific experimental requirements and compare images acquired with different objective lenses, for example, a higher NA 100× lens vs a 40× oil objective (Supplementary Fig. S4).

Using the proper coverslip is another important component of the optical path, since it will be placed between the sample and the objective lens. The coverslip is therefore included as part of lens design and impacts how light is focused on and collected from the sample. Deviations in coverslip thickness from the manufacturer's specification (typically No 1.5 for high NA lenses) can have a pronounced impact on image quality and data quantification, causing decreased resolution and contrast (Fellers and Davidson 2024). Even when using the proper coverslip, care must be taken that it is perpendicular to the objective, as tilted coverslips covering thick or uneven samples increase the apparent thickness of the coverslip and introduce asymmetrical aberrations and signal degradation.

Experimental design, image acquisition, and instrument settings

Experimental bias

When designing any experiment, steps should be taken to minimize bias. Experimental biases can affect experimental outcomes and compromise reproducibility, potentially leading to skewed data acquisition, analyses, and conclusions (Munafò et al. 2017; Lee et al. 2024). Biases during image acquisition emerge from two main sources: (1) sample bias, that is, when specific sections, regions, technical and/or biological replicates are selected for imaging; and (2) human/unconscious bias, that is, visual perception is biased toward the detection of certain features in a non-quantitative way and thus cannot provide reliable information (Brown 2017; Jost and Waters 2019; Jonkman 2020). Bias can be managed with good experimental design, which may include technical and biological replicates, use of appropriate controls, blinded/randomized samples, automated acquisition, and increased sample size using tiling and/or z-stack acquisition modes. Before acquisition, it is important to set up ways to track raw data, acquisition settings, image processing steps, and other parameters that will be required for analysis (Lee and Kitaoka 2018). Steps to limit biases, sample size, number of replicates, and any sample processing before imaging should be reported accurately when preparing images for publication.

Controls

Controls are required for the proper interpretation of any scientific data (Baker 1984; Lipsitch et al. 2010; Torday and Baluška 2019), and microscopy is no exception. While controls will be specific for each experiment, common themes emerge. As in any biological experiment, biotic, abiotic and/or chemical treatments need to be compared with mock treatment (i.e. vehicle only) and mutants need to be compared with wild-type control samples. However, imaging experiments also require additional controls. For example, the expression level of genetically encoded reporters (e.g. GFP-fusion proteins) can have a profound effect on their observed subcellular localizations (Lisenbee et al. 2003). Fusion proteins should be tested for functionality by their ability to complement corresponding mutant phenotypes, and it is best practice to confirm the molecular weight of the fluorescent protein-fusion protein via western blotting to ensure that the fluorophore is not cleaved from the protein of interest (Moore and Murphy 2009). When using affinity probes such as antibodies for immunolocalization (Baskin et al. 1992; Shimamura 2015; Guerin 2023a, 2023b), important negative controls include the use of non-immune serum, pre-immune serum (when available), and samples treated without a primary antibody but otherwise underwent all of the same processing steps as immunolabelled samples. For nucleic acid localization via in situ hybridization, a scrambled probe is an essential negative control (Prieto et al. 2007; Jiang 2019). Staining protocols should always compare stained samples to unstained controls to evaluate background signal and autofluorescence. Establishing an imaging pipeline with appropriate positive and negative controls is essential to obtain reliable, meaningful, and reproducible data to both enhance interpretation and assist in troubleshooting experimental anomalies.

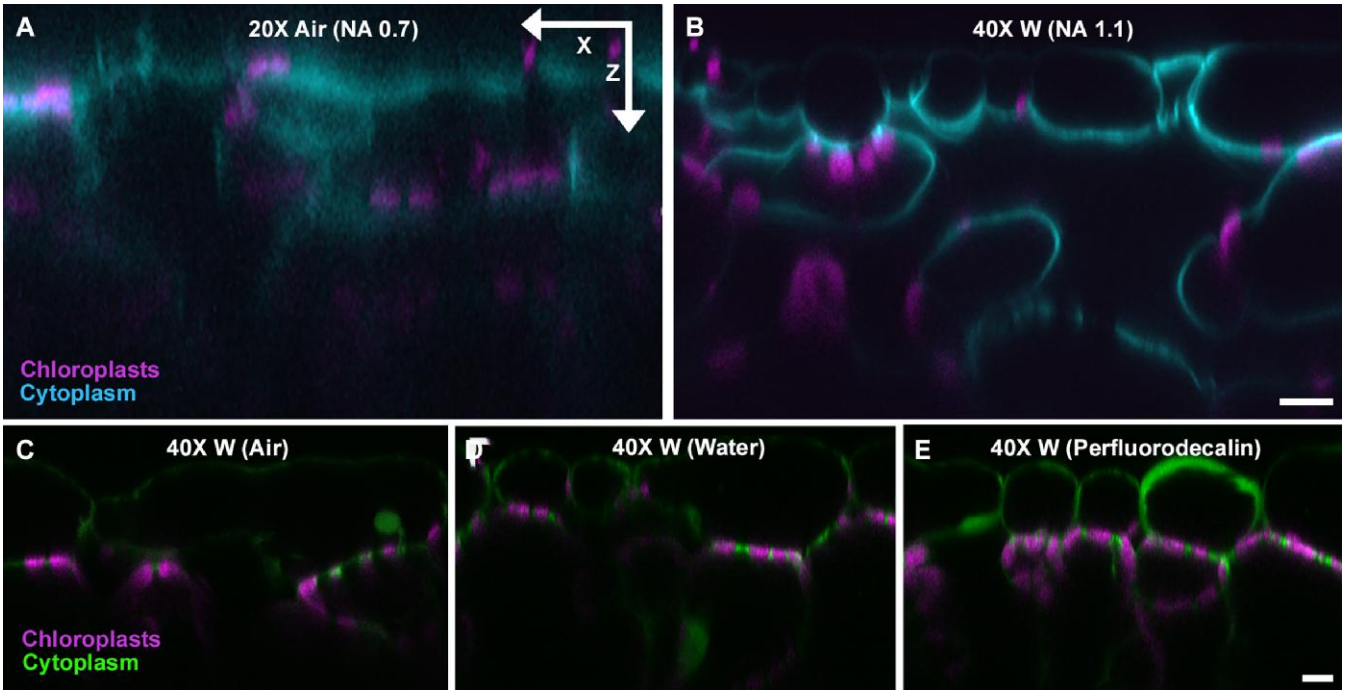

Figure 5. Comparison of objective lens and sample infiltration medium for live-cell imaging of *N. benthamiana* leaf epidermal and mesophyll cells. Single xz axis images of a tobacco leaf showed dramatically reduced image quality using a lower magnification/numerical aperture **A)** 20× air (NA 0.7) compared with a **B)** 40× water immersion (W) (NA 1.1) objective lens. Scale bar = 5 μm. Due to differences in spherical aberration, leaves that were mounted in water but not infiltrated to remove air spaces **C)** 40× W (air) exhibited reduced intensity and image quality, especially in deeper parts of the tissue, compared with water infiltrated leaves **D)** 40× W (water) or with best match of refractive index when using **E)** Perfluorodecalin infiltrated leaves (40× W; Perfluorodecalin). Cell cytoplasm, chlorophyll autofluorescence in chloroplasts. Refractive index of air = 1, water = 1.33, perfluorodecalin = 1.313. Scale bars = 10 μm.

Autofluorescence and imaging multiple fluorophores

Experimental conditions should also be established considering background autofluorescence and bleed-through. Plants produce many autofluorescent compounds—both generalized and environmentally induced and species/tissue specific. Autofluorescent compounds are often found in the cell wall, plastids or vacuole but may also be cytosolic. Common autofluorescent compounds in plant samples include cell wall lignin in the blue range (400 to 440 nm), chlorophyll in the red/far-red range (600 to 800 nm), and cell wall (grasses) or phloem (conifer) ferulic acid/ferulate in the blue range. (Donaldson 2020). Stressed or dying cells often produce secondary metabolites that autofluoresce in the cytosol or vacuole. We refer readers to a detailed list and associated spectra (Donaldson 2020). Autofluorescence will often appear in multiple channels, so checking for fluorescent signals across multiple channels will help identify if a signal is "real" and also identify the best wavelength range for the probe. To further discriminate between autofluorescence and "true" signals, appropriate controls should be used. For example, nontransgenic plants, when using genetically encoded fluorescent reporters (e.g. GFP) or unstained plants, when using dyes or immunofluorescence, should be imaged using identical acquisition settings. The mere presence of autofluorescence does not in itself prevent useful imaging results if proper controls are used; for example, strong fluorescence from the selected probe(s) can often overcome weak or tissue/organelle specific autofluorescence (Clancy and Cauller 1998; Piña et al. 2022). If the autofluorescence emission is at a wavelength that is not collected for other fluorophores in the experiment but provides useful cell structure markers (e.g. cell walls, vacuoles, chlorophyll etc.), it can provide useful context in imaging studies.

When using multiple fluorophores, an important control is to check for and apply strategies to minimize/eliminate bleed-through into other channels (Fig. 4), which can also result in misassignment of emission signals, and particularly false "co-localization." For example, many commonly used dyes, such as propidium iodide and FM4-64, have broad excitation and emission spectra that can be detected across multiple channels. Therefore, a useful approach is to image a specimen across multiple channels to determine if there is any channel bleed-through and then apply strategic selection of excitation wavelengths, sequential imaging and emission filters to limit any crosstalk (Fig. 4, C to F). The sequential excitation and emission strategy (1 fluorophore being excited and imaged at a time) along with judicious emission filter settings, is very effective to reduce/eliminate crosstalk of compatible multi-color fluorophore combinations (Fig. 4, C to F); however, sequential imaging will be slower compared with a simultaneous approach.

When planning to conduct fluorescent intensity measurements, best practice is to image a second fluorophore that should not change under experimental conditions. For example, nuclear-localized fluorescent proteins have been used as internal standards to conduct ratiometric measurements of fluorescent intensity of secreted GFP (Samalova et al. 2006) and during bimolecular fluorescence complementation experiments (Grefen and Blatt 2012). Autofluorescence can also be useful in this context.

Controls for live-cell imaging

Live cell imaging experiments need to be carefully monitored to avoid imaging dying or dead cells. Best practice includes imaging samples for the shortest possible time; however, with careful

sample preparation and appropriate controls, images can be collected over days or even weeks (Czymmek et al. 2004, 2007; Hervieux et al. 2016; Schneider et al. 2022; Gómez-Felipe et al. 2024; Le Gloanec et al. 2024). Environmental conditions should be monitored and controlled, including sample temperature and light conditions, since these can affect cellular dynamics and organization (Fujita et al. 2013; Lindeboom et al. 2013; Wang et al. 2020). Tissue dehydration can also adversely affect imaging, especially tissues without a waxy cuticle, such as roots. Although the signs of decreasing cell health can vary, some indicators of "dead cell imaging" include decreased or cessation of cytoplasmic streaming and Brownian motion (wiggling) of subcellular components (Chow et al. 2025); fragmentation of the plasma membrane, vacuole, ER network, and cytoskeletal networks; increased autofluorescence; or cessation of cellular growth. Vital stains can be used to determine whether cells remain alive during established imaging conditions; for example, although propidium iodide is a common counterstain for plant cell wall outlines, it will stain the cytoplasm and nuclei when the plasma membrane (cell viability) has been compromised (Hoffmann et al. 2024). Fluorescein diacetate or SYTOX^{T} dyes (Truernit et al. 2008) are other cell viability stains that can be effectively used in plants (Jones et al. 2016). Finally, when imaging cells and/or organs, especially for long imaging experiments, it is prudent to ensure imaging experiments do not alter sample biology. Best practice is to monitor a control specimen that is not subjected to the microscopy experiments to determine if there are differences in the size, shape, and developmental stage compared with the imaged specimen.

Instrument settings

Acquisition settings must be consistent when performing quantitative image comparisons. For example, if fluorescence intensity is being compared, the same microscope and acquisition settings (e.g. detector settings [offset/gain], pixel or frame exposure time, averaging, image size, filters, excitation power, objective lens) must be used to image control and test samples. Indeed, many commercial systems conveniently have a "reuse" (or equivalent) function to allow users to reload hardware/software settings from previously acquired data. Although convenient, not all settings may automatically be reapplied so the stored image metadata should be carefully compared with "reuse" settings for all imaging sessions.

There are dozens of instrument settings, many often not readily apparent, that can influence measurements for quantitative fluorescence microscopy such as system alignment or laser/light source stability (Pawley 2000). For system hardware, periodic system alignment, regular cleaning, and other tests using standard slides by the responsible core facility or system manager should be performed for quality control assessment of the imaging system. Recently, a kit for evaluating system performance has become available by loan from Bioimaging North America to assess and ensure reproducibility (Gaudreault et al. 2022; Nelson 2022; BINA 2024).

Background and dynamic range

Background signals are common in many imaging experiments and will vary by detector type. For example, widefield and spinning disk microscopes have cameras (rather than point detectors like PMTs, or comparable, which are common on LSCMs), and it is common to have gray rather than black (pixels with a zero-intensity value) backgrounds. There may be a temptation to adjust contrast (gain) and brightness (offset) settings, especially on LSCMs, to reduce/exclude background or unwanted signals, increase contrast or to emphasize a feature of interest. Image acquisition conditions should be adjusted to avoid excessive under- or over-saturated pixels (blue or red, respectively in (Fig. 6, C to E) to prevent "clipping" or truncation of the data, which can hinder reliable interpretation, cause loss of features, and compromise the ability to quantitatively analyze the image. During acquisition, this can be done by adjusting exposure/pixel dwell time, and or camera/detector contrast and brightness (gain and offset) settings. These same settings should be used to image all samples in a given experiment (i.e. wild type and mutant, or control and treatment). When first setting-up experimental conditions, we recommend leveraging the "range indicator" option available on many imaging systems that will apply a single color to represent black (e.g. blue assigned to 0 intensity pixels in an 8-bit image) and saturated/white pixels (e.g. red assigned to 255 intensity pixels in an 8-bit image), while all pixel intensities in between these extremes remain greyscale (Fig. 6, C to E). Alternatively, a histogram of the image can be generated, representing the pixel intensity distribution of the entire image (Fig. 6, C′ to E′), for experimental set-up or post processing to reveal "clipping." For quantitative settings across images, it is important that images reflect the truth in a comparable manner rather than offering an artistic or aesthetically pleasing image. For fluorescence quantification, images should only be acquired using consistent settings without over- and undersaturated pixels, as these pixels can skew the results. An exception to this rule is the acquisition of channels used to determine cell outlines for 2D/3D segmentation because many image analysis software packages can better detect cell outlines when the signal is strong (Wang et al. 2025).

Photobleaching

Even if settings are identical and the imaging system stable, other hardware dependent settings, such as the laser/light power at the sample, can adversely impact results. Notably, photophysical effects such as photobleaching can cause an irreversible loss of fluorescence due to a chemical modification of the fluorophore in the presence of light and free radical oxygen (Mahmoudian et al. 2011). These issues are especially problematic when collecting z-stacks or time-lapse experiments (compare Fig. 7, A and B with Fig. 7, C and D). While improved fluorophore design and free radical scavengers (anti-fade agents; see also Tips for working with fixed samples) help mitigate photobleaching, light/laser power and exposure/dwell time settings can also be adjusted to limit photobleaching depending on microscope platform. A quick check to assess photobleaching is to measure the intensity of the sample over time; nonlinear intensity-changes over time indicate that significant photobleaching is occurring (Fig. 7E). Photobleaching can be reduced by lowering the laser power (in this example, from 0.8% to 0.08%) and plotting intensity over time until average intensity remains constant over the expected imaging duration (Fig. 7E) and/or by decreasing image collection time, either by decreasing exposure time on camera-based systems or by increasing scan speed in LSCM systems. Additionally, cropping an image (scanning a smaller bounding area), while maintaining the same pixel resolution with point scanning microscopes, is an effective way to limit bleaching of larger tissue areas and increase scan rate. However, zooming to reduce scan area can potentially increase photobleaching and has a squared relationship to the zoom factor. For example, zooming from 1 to 2 concentrates the same amount of excitation light into one-fourth of the

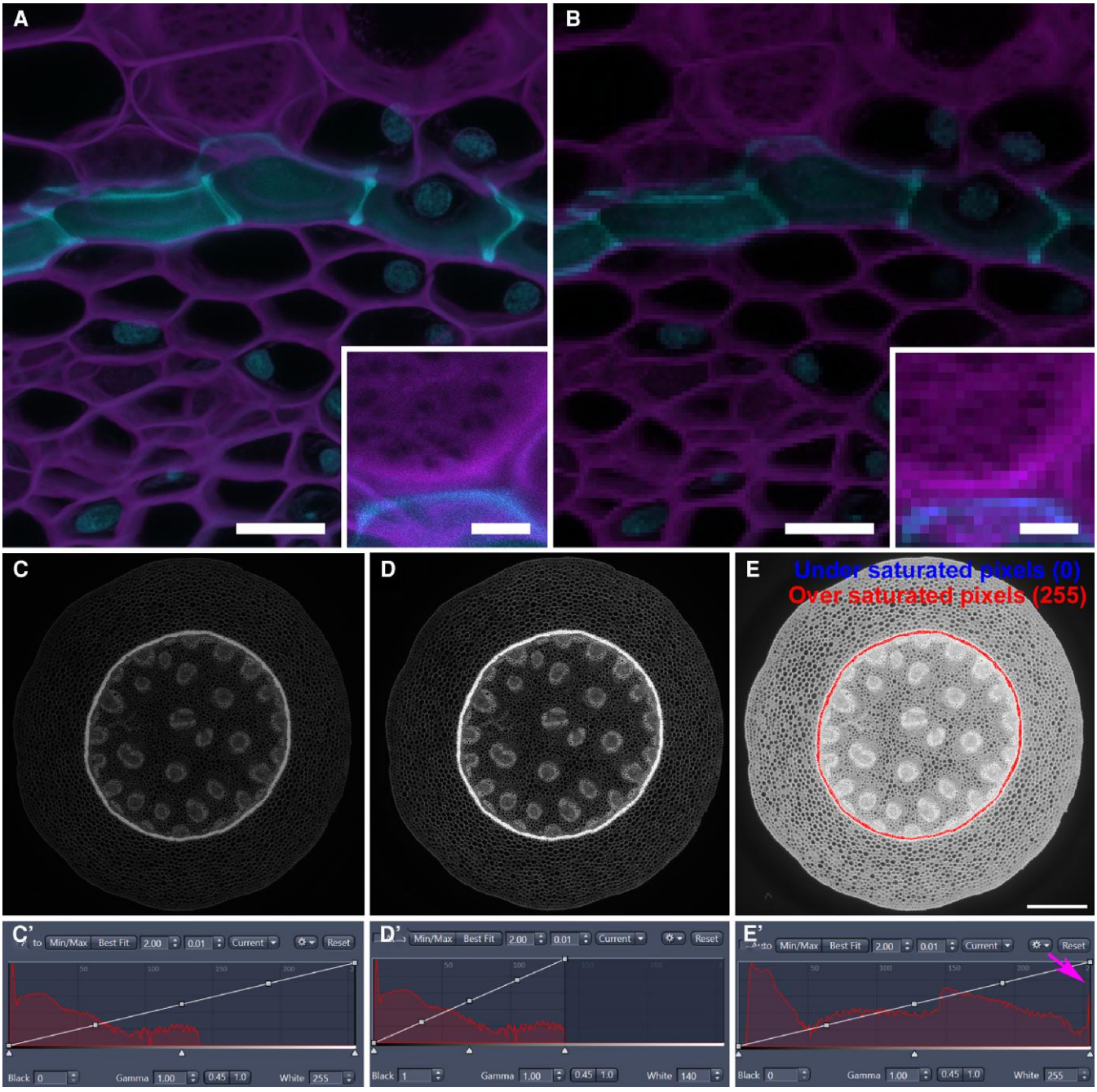

Figure 6. Pixel resolution and dynamic range on a test sample. **A)** An image of an acridine orange stained Convallaria stem section acquired at an image pixel number (2,048 × 2,048) and size (57 nm) that met Nyquist sampling requirements and achieved the best possible resolution for a 40× water (NA 1.1) objective lens. **B)** A comparison of the same location as **(A)** with reduced image pixel number (128×128) and size (918 nm) that did not meet Nyquist sampling but was acquired ~250 times faster. The acquisition conditions in **B)** would be sufficient to identify nuclei and measure cell area or shape, but not fine detail of the image (compare insets for magnified detail with/without Nyquist sampling conditions). Scale bars = 20 μm. Inset scale bars = 5 μm. **C)** The dynamic range of an 8-bit image can be assessed by viewing its corresponding histogram **C′)** and the dynamic range optimized for viewing and display by selecting min/max **D** and **D′)**. It is essential to avoid **E)** "clipping" the data (loss of information) by overexposure as evidenced with a range indicator to show any saturated pixels (E) or by reviewing the image histogram **E′)**, which showed stacking of pixels at the extremes (arrow). The Zeiss ZEN specific range indicator was applied in images C–E to show under and over saturated pixels, if any. Note: range indicator look-up tables will vary depending on software/vendor used. Scale bar = 500 μm.

area, zooming from 1 to 3 into one-nineth, etc. While lower excitation light and/or faster image collection will decrease signal-to-noise (image quality), keep in mind that noise is inherently present in all images; when the goal is to capture and measure a dynamic process or large volume, maintaining the integrity of the data should outweigh simply having an aesthetically pleasing dataset.

Objective vs pixel resolution

The resolution of a given objective lens is fixed and determined by its NA and the wavelength(s) of light being used, known as Rayleigh resolution limit (Pawley 2006). The theoretical Rayleigh lateral resolution for an objective lens for fluorescence is calculated as 0.61(λ)/NA, and for axial resolution (optical section thickness) as 1.67(λ)/(NA)^2 (Jonkman et al. 2003, 2020), where

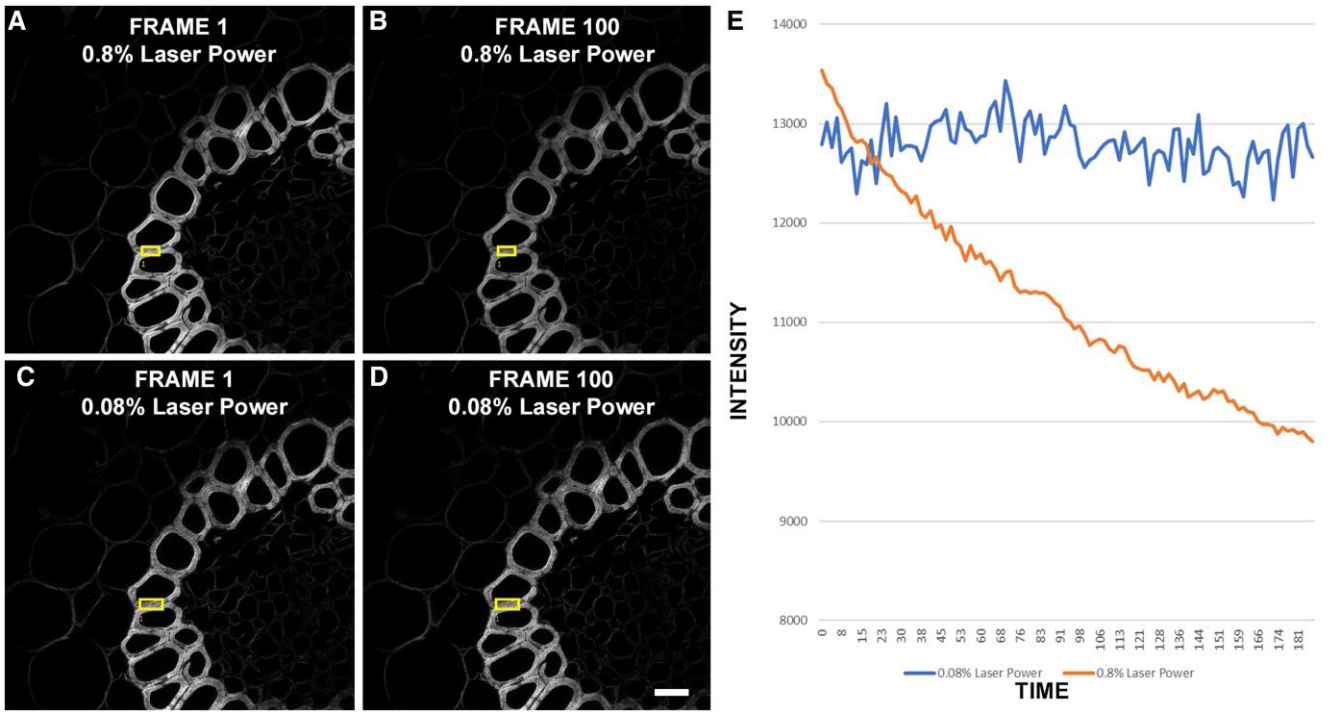

Figure 7. Effects of laser power on photobleaching. 100 frame time-lapse series of an acridine orange stained Convallaria stem section acquired over 185 s, at **A)** FRAME 1; **B)** final FRAME 100 at 0.8% laser power (488 nm) showed lower signal intensity in FRAME 100 compared with FRAME 1 due to photobleaching. Decreasing the laser power by 10-fold (0.08% laser power) showed comparable signal intensity in **C)** Frame 1; vs **D)** FRAME 100; **E)** Plotting the intensity over time in a region of the cell wall (box) in this sample showed that while the 0.08% laser power was noisier, it displayed minimal photobleaching compared with 0.8% laser power where the signal decreased about 30% in this ~185 s time-lapse. Scale bar = 20 μm.

λ = wavelength of the fluorophore. Thus, for a GFP fluorophore (530-nm peak emission) and 40× 1.1 NA lens, the Rayleigh resolution is calculated to be 294 nm and optical section thickness of 731 nm. However, depending on the number of final pixels in an image, often the full resolving power of the objective lens is not captured and may not always be needed. If the full resolution of the objective is required for an experiment, Nyquist sampling must be met, namely, there must be sufficient spacing of pixels in a 2D and/or 3D image to oversample the smallest resolvable structure by 2- to 4-fold (Pawley 2006). For example, a selected 2D field-of-view imaged with 2,048 × 2,048 pixels (pixel size 57 nm) meets the Nyquist sampling for the 40× 1.1 NA lens (Fig. 6A), while using 128 × 128 pixels (pixel size 918 nm) (Fig. 6B) falls far below and subtle features may be lost in an undersampled image. However, if the goal is simply to count the number of cells or measure cell perimeters, the smaller image size is perfectly adequate, has a smaller file size, and is ~250 times faster to collect. Undersampling also can be accomplished by increasing the scan speed by using a smaller frame size on a LSCM system, or by "binning" an EM-CCD (i.e. grouping a square of 2 × 2 adjacent pixels together into 1 larger pixel). Importantly, binning can also help with detection of weak signals. It is worth keeping in mind that most journals require 300 dots per inch pixel resolution for figures. Thus, a 512 × 512 pixel image will be ~1.7 ×1.7 inches at 300 dots per inch resolution, and this may be inadequate to display the desired feature without acquiring at greater pixel resolutions or interpolation (Fig. 6, A and B).

Image processing and analysis

Image processing and analysis are expansive topics and advanced image processing or analyses are beyond the scope of this primer. Processing and analysis can occur in a variety of software programs, including software that is used for acquisition (such as Nikon Elements, Leica LAS-X, Olympus FluoView, or ZEISS Zen), open source software such as ImageJ, specifically the Fiji distribution (Schindelin et al. 2012), or specialized software such as Imaris, Huygens (Day et al. 2017), CellProfiler (Stirling et al. 2021), or MorphoGraphX (Barbier de Reuille et al. 2015; Strauss et al. 2022). Here, we focus on the basics that every plant microscopist needs to address. We will briefly discuss common fundamentals but refer readers to several excellent general reviews that cover topics such as optimizing image acquisition settings, enhancing image quality, and performing basic measurements for data analysis (Russ 2006; Waters 2009; Bassel and Smith 2016; Hickey et al. 2021; Hobson et al. 2022).

Documenting processing steps

Image processing steps include anything that changes an image from its original form. These may include seemingly mundane changes such as adjustments to intensity (e.g. brightness/contrast), background subtraction or thresholding, smoothing or sharpening filters, applying lookup tables (false color of images), cropping, rotating, merging channels, changing bit-depth or resolution, creating z-projections or 3D reconstructions, and image compression, to name a few. It can also include more advanced processing, deconvolution, segmentation, or use of artificial intelligence with machine- or deep-learning approaches. Importantly, all of these image processing adjustments can alter the pixel values of images, which can dramatically affect any subsequent quantitative image analyses (Halazonetis 2005; Russ 2006). Understanding how detectors (Spring 2001) and processing steps can impact quantitative data will help microscopists make good

decisions about processing and analysis (Pawley 2006). For example, when exporting images to work with other software, many confocal microscopes acquire images with dynamic ranges of 8-bit (256 pixel gray levels), 12-bit (4,096 pixel gray levels), or 16-bits (65,536 pixel gray levels), while RGB color images are typically at least 24-bit (8-bits/channel, 16,777,216 colors). When given the choice, 16-bit images (or system maximum) are preferred, as images can be down-scaled to 8-bit for display purposes, but it cannot be reverted to 16-bit without loss of information. Likewise, when capturing and/or saving screenshots, color images are typically 8-bit RGB (only 256 total colors) and screenshots do not match the raw data pixel intensity values. Thus, conversion from 16- to 8-bit necessarily rescales the image. Also note that all detectors (point or camera-based) are simply collecting photons which are converted into a digital signal where the relative number of photons collected represents the intensity of the sample at a given position. RGB cameras use a color filter array and point detectors, such as PMTs, leverage user defined emission filters for each fluorescent channel. In either instance a look up table, black and white or color, is typically assigned to reflect the intensity range (Spring 2001). Quantification of pixel intensities must always be done on the original, full bit-depth images, and when converting to 8-bit for display, users should be aware of the image scaling impact. For example, Fig. 6, C and D shows an example of a single image acquired at one setting but displayed at different intensity scales. Digitally rotating images usually involves interpolating pixel information, which will also change pixel values. Assembling figures in PowerPoint or other presentation software, while convenient for presentations, has the risk of intentional or inadvertent changes in aspect ratio and image data compression, depending on settings. Likewise, converting images to different types (e.g. from TIFF to JPEG) to save disk space or for portability with other software results in lossy image compression, which will impact the quantitative and qualitative information in images (Fig. 8) and should only be used for presentations, websites, or communications where file size is limiting. An acceptable option, if space is a concern, is lossless compression formats of TIFF for multi-channel or z-stacks, or PNG files for single images. Overall, when comparing fluorescence intensity between samples, best practices include applying the same preparation steps to all samples, using the same acquisition settings to gather all data, and applying the same processing steps (avoiding irreversible file compression-based loss) to each image before data analysis.

Analysis routines can also range from simple to sophisticated and can be highly customized for specific applications. In general, image analyses involve extracting quantitative information from images, such as object size, object intensity, or the relationship between objects (e.g. ratiometric imaging (Samalova et al. 2006; Ast et al. 2017), colocalization (Lathe et al. 2024), or kymographs (Zhou et al. 2020; Verbančič et al. 2021). Since analyses rely on quantifying pixel/region intensity and/or coordinate values from images, and processing steps will change these values, it is best practice to conduct analyses on minimally processed or unprocessed images. It is also essential for users to report the software used (including version number) for image analyses, and all details of any segmentation and analysis steps applied (including parameters/settings in any algorithms applied), and how regions of interest were selected for analysis.

Image analysis in biological context

Plants have several unique features that should be specifically considered during image analyses. These include autofluorescence, rapid cytosolic streaming, and large central vacuoles. As discussed (see Autofluorescence and imaging multiple fluorophores), appropriate controls should be used to assess whether autofluorescence is contributing to the image and to minimize these contributions, especially for any quantitative analyses. For any live-cell imaging experiments, microscopists should consider whether rapid cytosolic streaming might be a confounding factor, since cellular contents can move at speeds up to 4.2 $\mu m\, s^{-1}$ (Nebenführ et al. 1999) which may be faster than the interval between images. In z-stacks, cytoplasmic streaming can alter the shape of objects, creating an elongated object (Nebenführ et al. 1999). In colocalization experiments, cytosolic streaming can decrease the degree of colocalization (Ebert et al. 2018). The large central vacuoles in many plant cell types, including protoplasts and *N. benthamiana* leaf epidermal cells, will push cytoplasmic contents to the edge of the cell, which can cause cytoplasm, ER, tonoplast membrane, or plasma membrane signals to be mistaken for each other (Fig. 9). Such mistakes can be avoided by colocalization of known markers with the construct of interest. Markers that positively identify many subcellular compartments with different fluorophores are available from stock centers (e.g. the Arabidopsis Biological Resource Center or Eurasian Arabidopsis Stock Centre) for a nominal fee as constructs for transient co-transformation (Nelson et al. 2007) or as stable Arabidopsis lines for crossing (Geldner et al. 2009). Alternatively, FM4-64 and PI counterstaining can differentiate between the plasma membrane and the cell wall, respectively, with some exceptions depending on tissue type and image modalities (Galvan-Ampudia et al. 2020). In either case, generating a line scan by drawing a line perpendicular to the plasma membrane and plotting fluorescent intensity of the marker compared with the probe of interest over the length of the line will illustrate whether the intensity peak of the signal of interest matches the intensity peak of the marker line or counterstain (Fig. 9, D to F, inserts). Z-stacks can also help to differentiate between different compartments, since ER-localized proteins will show characteristic web-like architecture in the cortical cytoplasm and peri-nuclear signal (Fig. 9, A to C).

Image manipulation, image integrity, and use of artificial intelligence

As discussed (see Experimental bias), human bias can be a large contributing factor in collecting and interpreting data. For microscopists this is further compounded in the digital era by the relative ease with which images can be adjusted, converted or otherwise modified in numerous places along a workflow. Indeed, it was reported that ~2% of accepted papers have either inappropriate modifications and/or manipulation, which can result in misrepresentation of the data (Cromey 2010; Martin and Blatt 2013) or insufficient reporting details (Marqués et al. 2020) Often in our experience, improper data handling can be unintentional and/or caused by lack of training. Furthermore, considering the power, potential, and rapid adoption of artificial intelligence (AI), a growing number of scientific hardware and software solutions (including generative AI) can automate finding, collecting, processing, segmenting, visualizing, and analyzing data (Wang et al. 2023). However, the same rules for data analysis and reporting apply when using AI. Namely, any approach that modifies or processes data, AI or other, must be accounted for, users should understand the consequences of these analyses and all processing steps must be reported with sufficient detail to ensure reproducibility. Furthermore, since AI models and training data are evolving rapidly, simply using the same tool does not assure reproducible analyses, especially when using proprietary or otherwise opaque image processing algorithms, and results may vary unless the

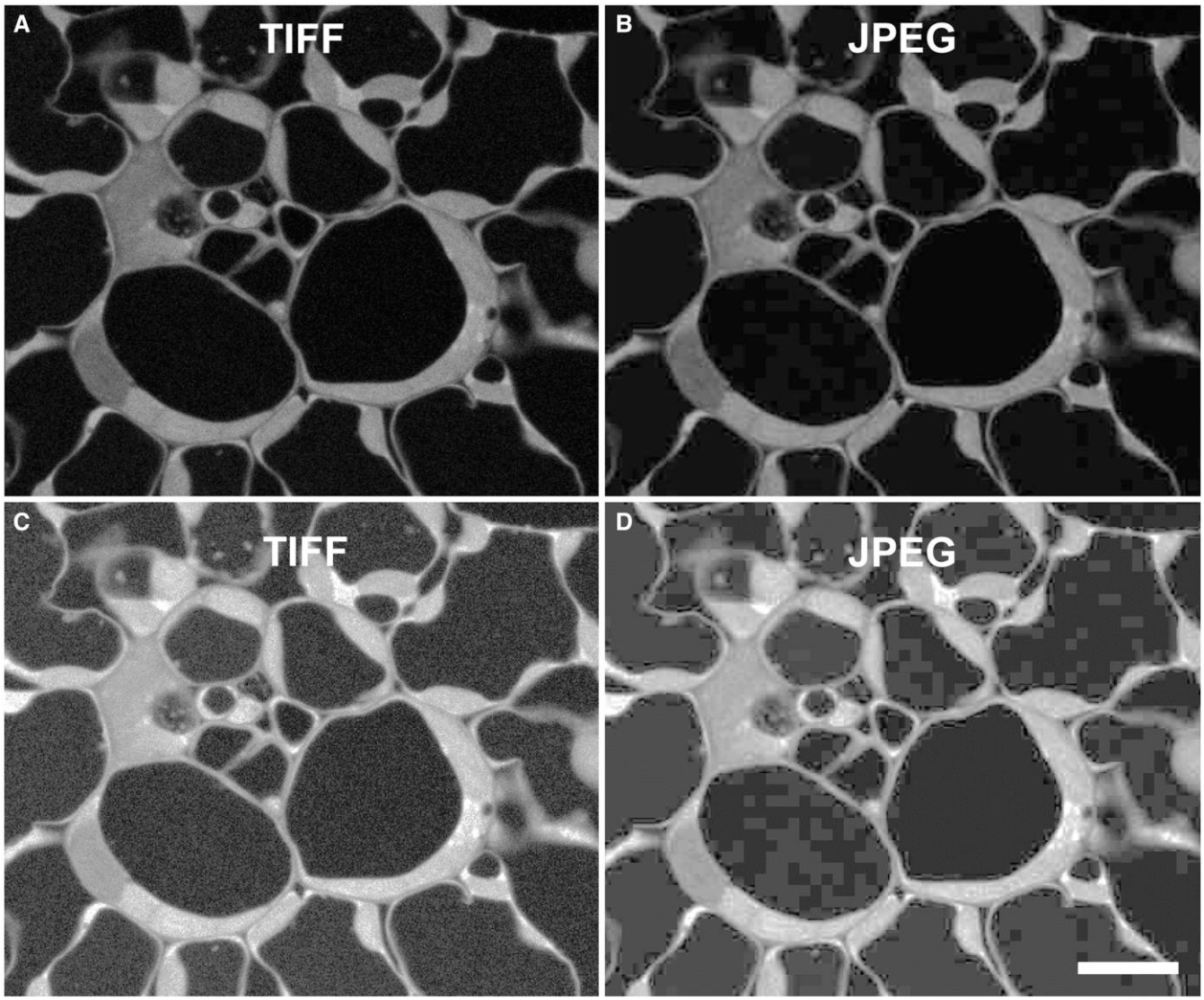

Figure 8. Image formats and lossless (TIFF) vs lossy (JPEG) compression. **A)** A 1,024- × 1,024-pixel image of an acridine orange stained Convallaria stem section saved as TIFF compared with JPEG compression **B)**. **C)** Increasing the image brightness of the TIFF image **(A)** showed fine texture in vacuoles and no detail loss. **D)** Increasing the image brightness of the JPEG image **(B)** revealed numerous artifacts and edge effects from the altered/compressed pixels making this data impossible to reliably quantify. Scale bar = 20 μm.

same version is used and/or a fixed model and training data are used for processing and all analyses.

Image annotation and presentation

The specifications of figure assembly are typically provided by each journal, but microscopists must make many decisions about how to display and communicate data. Researchers have created community-driven checklists to improve the quality and reporting of microscopy images in publications (Schmied et al. 2024). These resources offer practical guidance on image preparation, including formatting, color choices, and data sharing, as well as best practices for describing image analysis workflows. Basic image annotations should always include scale bars, plus time stamps, if applicable. If multiple images are to be compiled and compared (e.g. wild type vs mutant) matched magnification and a common scale is best. Insets or additional panels, either showing a tissue overview or a zoomed-in view may help orient the reader or highlight elements of interest at increased detail. Similarly, if a z-projection is being performed and images are being compared, the same method (e.g. maximum intensity projection) must be used, and the number of planes projected should be reported and ideally the same amongst samples. When displaying a single channel and/or transmitted light, side-by-side grayscale images are best, as we have done herein (Figs. 6 and 9). When displaying multi-channel or multi-color images, application of a cyan, yellow, magenta, green, and/or grayscale color-schemes are the most accessible to readers and avoid using a combination of colors that are indistinguishable for color blind people (Jambor et al. 2021); we have provided several different examples of suitable color combinations throughout this manuscript.

Reporting

FAIR principles and public repositories

Comprehensive reporting is essential for accurate research communication, reproducibility, and data accessibility/reusability. Findability, accessibility, interoperability, and reusability (FAIR)

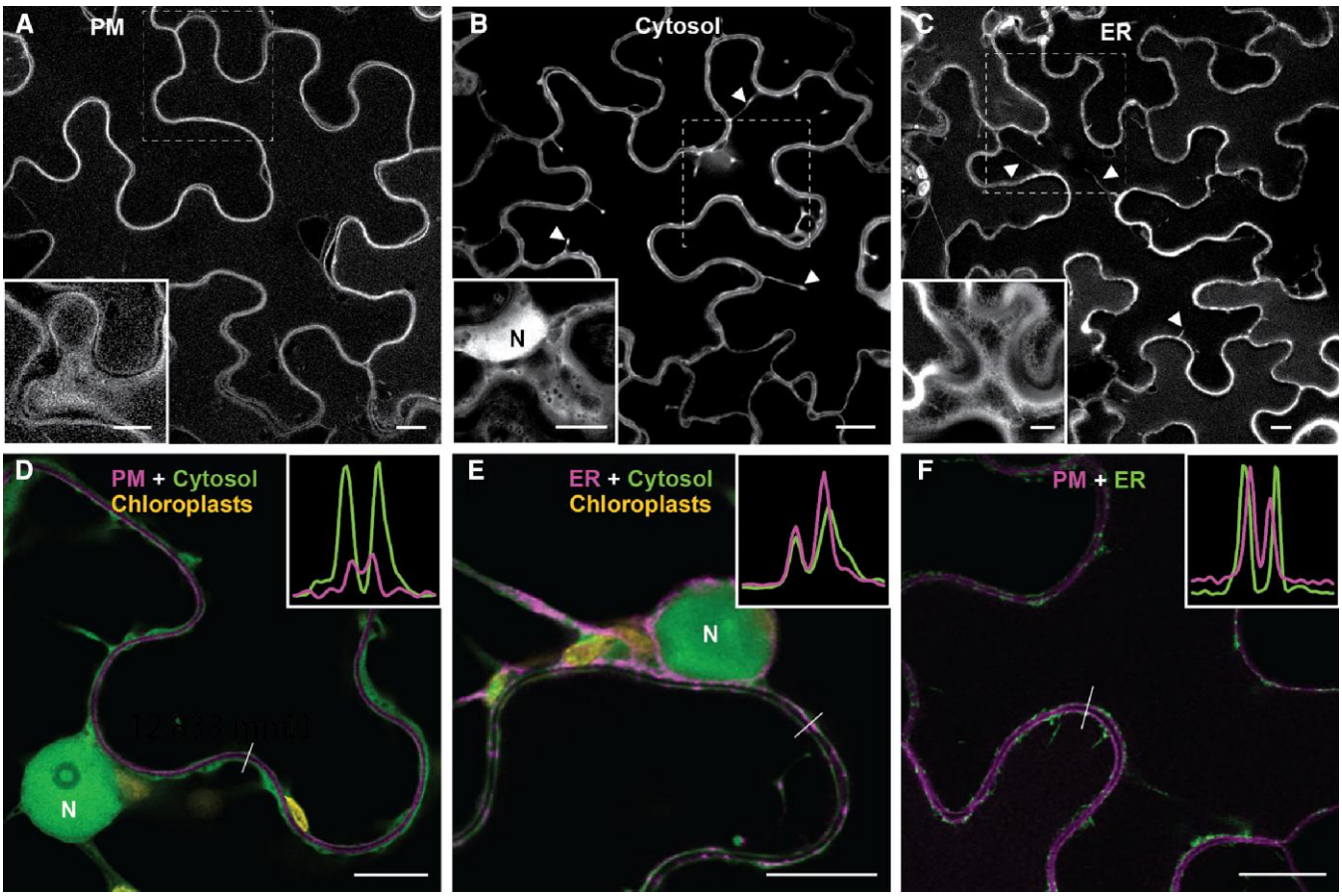

Figure 9. Distinguishing different membranes in plant cells. **A-C)** Mid-plane view and insert of cortical view of *N. benthamiana* leaf epidermal cells transiently transformed with plasma membrane (PM) marker, PIP2A-mCherry (pm-RK; Nelson et al. 2007) **A)**; cytosolic marker, untagged GFP **B)**, and the synthetic mCherry-tagged endoplasmic reticulum (ER) marker er-RB (Nelson et al. 2007) **C)**. The main panels show a cell around its mid-point, while the insets show a region of the same cell but close to its cortex. The dotted lines mark the areas shown in inserts. Arrowheads indicate transvacuolar strands. **D-F)** Border regions between *N. benthamiana* leaf epidermal cells transiently co-expressing markers for PM (pm-RK, magenta) plus cytosol (untagged GFP, green) **D)**, ER (er-RB) plus cytosol (untagged GFP) **E)**, and plasma membrane (pm-RK) plus ER (er-GB) **F)**. Inserts show line scan analyses for the white lines drawn in the main panels. The X-axis of the graph corresponds to the position along the line (the total line length is 4.2, 3.5, and 4.9 μm in **D**-**F**, respectively), while the Y-axis shows the fluorescent intensity for both channels at each point along the line. Note the differences in the relative position of the peaks from the 2 channels. All images were subjected to deconvolution using Olympus FluoView software. N, nucleus; Scare bars = 10 μm.

guiding principles outline best practices for data management (Wilkinson et al. 2016). Unfortunately, microscopy methods and micrograph analyses are often vaguely or incompletely described in publications (Marques et al. 2018; Heddleston et al. 2021; Montero Llopis et al. 2021). The responsibility to improve reporting lies with authors, reviewers, editors, and ultimately with scientific journals. Indeed, several journals have recently updated guidelines for light microscopy-related reporting (https://doi.org/10.1038/s41556-025-01704-y; https://doi.org/10.1038/s41594-025-01605-6). However, we recognize that the complexities of these considerations may be daunting for novice microscope users or non-expert reviewers. As a companion, and not replacement for written materials and methods, we provide a straightforward reporting spreadsheet template (Supplementary Table S1) that can be used as a convenient approach to manage details about the samples and imaging setup for each figure. Excellent alternatives are also available to meet diverse lab needs (Heddleston et al. 2021) (https://doi.org/10.1038/s41556-025-01704-y; https://doi.org/10.1038/s41594-025-01605-6). Ideally, all corresponding original raw data underlying images in the vendor's native format and methods are deposited in an open and public data repository, such as Zenodo (Sicilia et al. 2017) or Open Science Framework (Foster and Deardorff 2017). Depending on file size and data type, other publicly funded repositories such as BioImage Archive (Hartley et al. 2022) or Electron Microscopy Public Image Archive (Iudin et al. 2016, 2023) may be appropriate. Sharing data via repositories also permits data reuse or meta-analyses by the community. An unambiguous organizational schema for image classification that includes sample type (plant, tissue, and cell type), fluorophore/stain, instrument and image acquisition parameters, and any processing steps can facilitate data reuse. While this framework for representing fluorescence imaging data does not currently exist in a mature form and data size is still an issue, other databases, such as the Protein Data Bank (Burley et al. 2019), may offer useful lessons for establishing community driven data frameworks, similar to the macromolecular Crystallographic Information Framework, the data standard for structural biology (Westbrook et al. 2022). For now, accurate recording and reporting of all imaging experiment steps promotes reproducibility and can support troubleshooting when experimental outcomes vary or are unexpected. Importantly, good reporting goes hand-in-hand with thoughtful experimental design and recording from the very beginning of the process, thus we recommend consulting the reporting spreadsheet template (Supplementary Table S1) (or a similar alternative) prior to starting each experiment and while conducting experiments.

Sample treatment and microscope settings

As discussed above, many factors can dramatically influence microscopy data and these must all be reported. For example, the specific fluorophore used or manufacturer and catalog number of any antibodies or dyes must be reported since their spectral and binding properties can vary greatly. Likewise, for fixed samples, a detailed protocol will include manufacturer and catalog numbers for all reagents plus concentration and timing for key steps, such as fixation, washes with buffers and incubation with antibodies. For live cell imaging, environmental conditions during the experiment can have a strong effect on plant cells and the biological phenomenon being studied, including ambient temperature and light conditions, and/or how live tissues were oriented relative to the gravity vector (von Wangenheim et al. 2017) (Supplementary Fig. S5), so these should also be reported. Similarly, microscope characteristics and settings such as imaging modalities, objective properties, excitation and emission optics, and image collection parameters must be reported (Supplementary Table S1).

Image analysis and statistics

Image analysis details must also be reported since software for image processing is constantly evolving. In general, the program/software must be reported (manufacturer and/or citation to publication, including version number), as well as any details of the algorithms applied to the images and the parameters/settings used for application of these algorithms. Some examples include details of brightness and contrast adjustments, background subtraction, denoising, deconvolution, thresholding, and segmentation (Aaron and Chew 2021). Sufficient detail for reproducibility should be provided for any quantification, such as which tissues and cell types were used for quantification, how features were selected for measurements, and how the sample size was calculated. *P*-values are often dramatically overestimated in microscopy experiments (also called "p-hacking") by measuring multiple events/objects from a single biological organism or cell but counting each of these events/objects as independent biological replicates (Lord et al. 2020). For example, if 10 plastids were measured from 1 control plant and 10 plastids were measured from 1 inhibitor-treated plant, then $n = 1$ for each condition, since differences in the plastids could simply be due to natural variation between the plants, location in the plant or due to the inhibitor treatment (Lord et al. 2020). Many commonly used statistical tests, including the *t* test, are sensitive to sample size and data distribution, so oversampling each biological replicate and therefore artificially inflating sample size can dramatically skew conclusions from statistical analyses and data that do not fit a normal distribution may need to be compared via alternative statistical tests. Best practices include clearly defining sample size in methods and figure legends, defining sample size as the number of independent biological replicates, testing data for assumptions of common statistical tests (e.g. normality, equal variance), using appropriate statistical analyses, and plotting data in a transparent fashion (e.g. using a plot type that displays all data points along with summary statistics).

Figure/results presentation

While each journal will have individual requirements for figure preparation, several steps are universal when preparing microscopy figures for publication. Figure and movie legends must include essential information for interpretation, such as scale bars, time stamps, and calibration bars for any non-linear lookup tables (false-coloring of images). Figure legends should also contain clear information about the cell type and developmental stage observed, as well as an indication of whether images are single frame or a projection (e.g. a maximum intensity projection of a z-stack or sum projection of a time series). When direct comparisons are being made between wild type and mutant, or treatment and control, control and experimental images should be displayed in the same fashion.

While the complete list of factors that must be reported for any microscopy experiment can seem overwhelming, appropriate methods reporting facilitates research communication, experimental reproducibility, and data accessibility. Therefore, we urge authors and reviewers to make use of the reporting spreadsheet template provided here (Supplementary Table S1) and suggest that scientists collect this information as they conduct their experiments to ensure that microscopy methods are appropriately reported in any resulting publication. While reporting can be complex, regularly updating conventional or electronic lab notebooks through the entire process simplifies data analysis, data interpretation and manuscript preparation (Buckholt and Rulfs 2022).

Conclusion

Many factors are involved in obtaining robust and meaningful results when applying fluorescence imaging across diverse scientific questions in plant research. While not exhaustive, the goal of this primer was to bring attention to and provide a guide through some of the most common challenges that arise in plant fluorescent imaging experiments from experimental design to publication. Many common pitfalls in plant imaging can be simply remedied through awareness and training. Ultimately, imaging data can be obtained in many different ways but depending on the experimental goal and how data were acquired, there can be limitations on meaningful interpretation and quantitative results due to lack of adequate documentation and reporting. More importantly, in an effort toward transparency and following FAIR principles we urge the plant science community to accelerate improvements in quality control, efficiency, reproducibility, data availability, and biological insights by adopting these best practices in plant fluorescence imaging.

Funding

The Plant Cell Atlas Initiative was funded by Research Coordination Network Award from the National Science Foundation (Award # MCB 2052590 and MCB 2420369) to Dr. Seung Rhee. H.E.M. is the Canada Research Chair in Plant Cell Biology. Some imaging was conducted using instruments supported by Canada Foundation for Innovation and the Ontario Research Fund: Research Infrastructure grants (38721) to H.E.M. This work was supported in part by the Natural Sciences and Engineering Research Council of Canada NSERC Discovery Grant (2020-05959) and an Ontario Early Researcher Award (ER21-16-256) to H.E.M. K.J.C. acknowledges imaging support from the Advanced Bioimaging Laboratory (RRID:SCR_018951) at the Danforth Plant Science Center and usage of the Leica SP8-X confocal microscope acquired through an Major Research Instrumentation grant from the National Science Foundation (DBI-1337680) and the ZEISS Elyra 7 Super-Resolution Microscope acquired through an Major Research Instrumentation grant from the National Science Foundation (DBI-2018962). D.K. was supported by the Natural Sciences and Engineering Research Council of Canada NSERC Discovery Grant (RGPIN-2018-04897). G.D. acknowledges support in part through access to the UC

Davis MCB Light Microscopy Core Facility and the Shared Instrumentation Grant Program from the National Institutes of Health (S10OD026702) for funding of the Zeiss 980 LSM and training and support by Dr. Thomas Wilkop. Y.B.-A. work is supported by the United Kingdom Research and Innovation (UKRI) council Future Leaders Fellowship (MR/T04263X/1).

Supplementary data

The following materials are available in the online version of this article.

All original raw microscope image data (Figs. 3 to 6, 7 to 9, Supplementary Figs. S3 and S4 and S5) are available as a public repository at Zenodo (10.5281/zenodo.14895059).

Supplementary Figure S1. A simplified upright fluorescence microscopy light path. The light source is directed through a dichroic filter cube which contains an excitation filter, a dichroic mirror, and an emission filter. The excitation filter is used to select the excitation wavelength and the dichroic mirror reflects the light through to the objective lens, which acts as a condenser, focusing the light into the specimen. Fluorescence emission signals will be generated at longer wavelengths which pass back through the objective lens and then are transmitted through the dichroic mirror and emission filter. The emission filter is used to define what wavelengths match the target signal (e.g. GFP) and the signal is collected by the detector (e.g. camera, photomultiplier tube or other).

Supplementary Figure S2. Low-cost method of sample preparation of leaf tissue. (A) A 6-mm biopsy punch, 10-mL syringe, and parafilm strips (B). C) Using proper PPE, use a 6-mm biopsy punch and rubber stopper behind the leaf to remove leaf disks (D). (E) Add or draw up water, buffer, or buffer with stain into the syringe to desired level, remove the plunger (F), add leaf disks, replace plunger, and, while orienting the syringe with tip upward (H), carefully push out any trapped air. Note the leaf disk has a light coloration due to air within the mesophyll. While pressing at the syringe tip with an index finger to close off the aperture, gently pull the syringe plunger to create a vacuum and note air bubbles coalescing on the leaf surface (I), release the index finger and the surrounding solution will enter the leaf, replacing the air spaces (J). Repeat the cycles a few times until the entire leaf darkens (K). (L) Using double-sided adhesive spaces, (M) mount onto a standard glass slide. (O) Add a small drop of water/buffer solution to the center of the well, (P) place the leaf disk onto the drop in desired orientation (e.g. adaxial/or abaxial facing up). To minimize air trapped between the coverslip and leaf surface, (Q) place a small drop of solution on a 22- × 30-mm coverslip, quickly invert, (R) align, and (S) place the coverslip onto the adhesive chamber and gently press along edges to seal. (T) Inspect to ensure minimal air bubbles between the tissue and the coverslip. Small bubbles adjacent to the leaf disk are acceptable if not interfering with leaf surface imaging.

Supplementary Figure S3. Quantitative imaging of thick samples can be impacted by objective lens choice. This objective comparison showed XZ axis images that extended from the coverslip (top) to ~300 μm z-depth (bottom) of a FITC infiltrated agar slab with similar optical properties to living tissue. Each hash mark represents 50 μm. Signal Intensity using a low magnification/numerical aperture 10× air (NA 0.3) or intermediate magnification/numerical aperture water immersion 40× water (NA 1.1) was greater and more uniform with increased depth than the 20× air (NA 0.70) or 100× oil (NA 1.4) largely due to spherical aberration. However, the 100× NA 1.4 lens outperforms these other lenses in resolution when imaging very near the coverslip.

Supplementary Figure S4. 40× and 100× oil objective lens comparison of *A. thaliana* root division zone epidermal cells using spinning disk confocal microscopy. (A) Overview and (B) digital zoom image of *A. thaliana* root imaging of membrane stain, FM4-64 (magenta), and Syntaxin of Plants SYP61 CFP-SYP61 (cyan) collected with a 40× NA 1.3 oil immersion objective. (C) Under the same acquisition settings as (A) but using a 100× NA 1.49 oil immersion objective, a notable loss in signal strength (compare A and C) but rescaling of the histogram (D) showed an increase in contrast and cellular detail (resolution) of CFP-SYP61 vesicles. (A) Scale bar = 20 μm, (B-D) Scale bar = 10 μm.

Supplementary Figure S5. Dynamics of gravi-dependent amyloplast sedimentation in Arabidopsis primary roots. (A) Overview of a vertically mounted Zeiss LSM800 confocal microscope compared with a horizontal stage microscope (B) used to image the Arabidopsis transgenic marker line (Pt-YK) expressing YFP tagged plastids counterstained with propidium iodide (magenta) for analysis of gravity-dependent statolith sedimentation. (C) Dense starch filled amyloplasts (green) sediment towards the physical bottom of gravity sensing columella cells in Arabidopsis primary roots. (D) In gravistimulated roots, the sedimentation of these amyloplasts (indicated by white arrowheads) towards the new physical bottom of these cells can be clearly visualized when imaged with a vertical confocal microscope. (E) However, the dynamics of amyloplast sedimentation are lost when images are captured with a conventional horizontal microscope. Scale bar = 20 μm.

Conflict of interest statement. None declared.

Data availability

All original raw microscope image data (Figs. 3, 5 to 9, Supplementary Figs. 3 to 5) are available as a public repository at Zenodo (10.5281/zenodo.14895059).

References

Aaron J, Chew T-L. A guide to accurate reporting in digital image processing—can anyone reproduce your quantitative analysis? *J Cell Sci*. 2021:134(6):jcs254151. https://doi.org/10.1242/jcs.254151

Abramowitz M, Davidson M. Microscope objectives—immersion media; 2015 [accessed 2025 Jun 19]. https://micro.magnet.fsu.edu/primer/anatomy/immersion.html

Ast C, Foret J, Oltrogge LM, De Michele R, Kleist TJ, Ho C-H, Frommer WB. Ratiometric matryoshka biosensors from a nested cassette of green- and orange-emitting fluorescent proteins. *Nat Commun*. 2017:8(1):431. https://doi.org/10.1038/s41467-017-00400-2

Aswani K, Jinadasa T, Brown CM. Fluorescence microscopy light sources. *Micros Today*. 2012:20(4):22–28. https://doi.org/10.1017/S1551929512000399

Baker R. The controlled experiment in the scientific method with special emphasis on biological control. *Phytopathology*. 1984:74(9):1019. https://doi.org/10.1094/Phyto-74-1019

Balcerowicz M, Shetty KN, Jones AM. Fluorescent biosensors illuminating plant hormone research. *Plant Physiol*. 2021:187(2):590–602. https://doi.org/10.1093/plphys/kiab278

Barbier de Reuille P, Routier-Kierzkowska A-L, Kierzkowski D, Bassel GW, Schüpbach T, Tauriello G, Bajpai N, Strauss S, Weber A, Kiss A, et al. MorphoGraphX: a platform for quantifying morphogenesis in 4D. *eLife*. 2015:4:e05864. https://doi.org/10.7554/eLife.05864

Baskin TI, Busby CH, Fowke LC, Sammut M, Gubler F. Improvements in immunostaining samples embedded in methacrylate: localization of microtubules and other antigens throughout developing

organs in plants of diverse taxa. *Planta*. 1992:187(3):405–413. https://doi.org/10.1007/BF00195665

Bassel GW, Smith RS. Quantifying morphogenesis in plants in 4D. *Curr Opin Plant Biol*. 2016:29:87–94. https://doi.org/10.1016/j.pbi.2015.11.005

Bell K, Mitchell S, Paultre D, Posch M, Oparka K. Correlative imaging of fluorescent proteins in resin-embedded plant material. *Plant Physiol*. 2013:161(4):1595–1603. https://doi.org/10.1104/pp.112.212365

Berg RH, Beachy RN. Fluorescent protein applications in plants. *Methods Cell Biol*. 2008:85:153–177. https://doi.org/10.1016/S0091-679X(08)85008-X

BINA (Bioimaging North America). Metrology Suitcase. 2024 [accessed 2025 Jun 19]. https://www.bioimagingnorthamerica.org/metrology-suitcase/

Brown DL. Bias in image analysis and its solution: unbiased stereology. *J Toxicol Pathol*. 2017:30(3):183–191. https://doi.org/10.1293/tox.2017-0013

Buckholt MA, Rulfs J. Electronic laboratory notebook use supports good experimental practice and facilitates data sharing, archiving and analysis. In: Pelaez TR, Gardner NJ, Anderson SM, editors. *Trends in teaching experimentation in the life sciences. Contributions from Biology Education Research*. Cham: Springer; 2022. p. 415–440.

Burley SK, Berman HM, Bhikadiya C, Bi C, Chen L, Di Costanzo L, Christie C, Duarte JM, Dutta S, Feng Z, et al. Protein data bank: the single global archive for 3D macromolecular structure data. *Nucleic Acids Res*. 2019:47(D1):D520–D528. https://doi.org/10.1093/nar/gky949

Campbell RE, Tour O, Palmer AE, Steinbach PA, Baird GS, Zacharias DA, Tsien RY. A monomeric red fluorescent protein. *Proc Natl Acad Sci U S A*. 2002:99(12):7877–7882. https://doi.org/10.1073/pnas.082243699

Celler K, Fujita M, Kawamura E, Ambrose C, Herburger K, Holzinger A, Wasteneys GO. Microtubules in plant cells: strategies and methods for immunofluorescence, transmission electron microscopy, and live cell imaging. *Methods Mol Biol*. 2016:1365:155–184. https://doi.org/10.1007/978-1-4939-3124-8_8

Chow F, Mohammad E, McFarlane HE. Protocol for detecting intracellular aggregations in Arabidopsis thaliana cell wall mutants using FM4-64 staining. *STAR Protoc*. 2025:6(1):103665. https://doi.org/10.1016/j.xpro.2025.103665

Chu KL, Koley S, Jenkins LM, Bailey SR, Kambhampati S, Foley K, Arp JJ, Morley SA, Czymmek KJ, Bates PD, et al. Metabolic flux analysis of the non-transitory starch tradeoff for lipid production in mature tobacco leaves. *Metab Eng*. 2022:69:231–248. https://doi.org/10.1016/j.ymben.2021.12.003

Clancy B, Cauller L. Reduction of background autofluorescence in brain sections following immersion in sodium borohydride. *J Neurosci Methods*. 1998:83(2):97–102. https://doi.org/10.1016/S0165-0270(98)00066-1

Clark NM, Hinde E, Winter CM, Fisher AP, Crosti G, Blilou I, Gratton E, Benfey PN, Sozzani R. Tracking transcription factor mobility and interaction in Arabidopsis roots with fluorescence correlation spectroscopy. *eLife*. 2016:5:e14770. https://doi.org/10.7554/eLife.14770

Colin L, Martin-Arevalillo R, Bovio S, Bauer A, Vernoux T, Caillaud M-C, Landrein B, Jaillais Y. Imaging the living plant cell: from probes to quantification. *Plant Cell*. 2022:34(1):247–272. https://doi.org/10.1093/plcell/koab237

Collins TJ. Mounting media and antifade reagents. *Microsc Today*. 2006:14(1):34–39. https://doi.org/10.1017/S1551929500055176

Conéjéro G, Noirot M, Talamond P, Verdeil J-L. Spectral analysis combined with advanced linear unmixing allows for histolocalization of phenolics in leaves of coffee trees. *Front Plant Sci*. 2014:5:39. https://doi.org/10.3389/fpls.2014.00039

Cox KL, Pardi SA, O'Connor L, Klebanovych A, Huss D, Nusinow DA, Meyers BC, Czymmek KJ. ExPOSE: a comprehensive toolkit to perform expansion microscopy in plant protoplast systems. *Plant J*. 2025:121(5):e70049. https://doi.org/10.1111/tpj.70049

Cromey DW. Avoiding twisted pixels: ethical guidelines for the appropriate use and manipulation of scientific digital images. *Sci Eng Ethics*. 2010:16(4):639–667. https://doi.org/10.1007/s11948-010-9201-y

Czymmek KJ, Fogg ML, Sweigard JA, Kang S. In vivo microscopy of vascular wilt disease in *Arabidposis thaliana*. *Microsc Microanal*. 2004:10(S02):216–217. https://doi.org/10.1017/S1431927604882503

Czymmek KJ, Duncan KE, Berg H. Realizing the full potential of advanced microscopy approaches for interrogating plant-microbe interactions. *Mol Plant Microbe Interact*. 2023:36(4):245–255. https://doi.org/10.1094/MPMI-10-22-0208-FI

Czymmek KJ, Fogg M, Powell DH, Sweigard J, Park S-Y, Kang S. In vivo time-lapse documentation using confocal and multi-photon microscopy reveals the mechanisms of invasion into the Arabidopsis root vascular system by fusarium oxysporum. *Fungal Genet Biol*. 2007:44(10):1011–1023. https://doi.org/10.1016/j.fgb.2007.01.012

Davidson MW, Dailey ME, Shaw SL, Swedlow JR, Andrews PD, Langhorts MF. *ZEISS campus: education in microscopy and digital imaging*; 2024 [accessed 2025 Jun 19]. https://zeiss-campus.magnet.fsu.edu/articles/livecellimaging/techniques.html

Day KJ, La Rivière PJ, Chandler T, Bindokas VP, Ferrier NJ, Glick BS. Improved deconvolution of very weak confocal signals. *F1000Res*. 2017:6:787. https://doi.org/10.12688/f1000research.11773.1

Diel EE, Lichtman JW, Richardson DS. Tutorial: avoiding and correcting sample-induced spherical aberration artifacts in 3D fluorescence microscopy. *Nat Protoc*. 2020:15(9):2773–2784. https://doi.org/10.1038/s41596-020-0360-2

Donaldson L. Autofluorescence in plants. *Molecules*. 2020:25(10):2393. https://doi.org/10.3390/molecules25102393

Duncan KE, Czymmek KJ, Jiang N, Thies AC, Topp CN. X-ray microscopy enables multiscale high-resolution 3D imaging of plant cells, tissues, and organs. *Plant Physiol*. 2022:188(2):831–845. https://doi.org/10.1093/plphys/kiab405

Duwé S, Dedecker P. Optimizing the fluorescent protein toolbox and its use. *Curr Opin Biotechnol*. 2019:58:183–191. https://doi.org/10.1016/j.copbio.2019.04.006

Dyachok J, Sparks JA, Liao F, Wang Y-S, Blancaflor EB. Fluorescent protein-based reporters of the actin cytoskeleton in living plant cells: fluorophore variant, actin binding domain, and promoter considerations. *Cytoskeleton*. 2014:71(5):311–327. https://doi.org/10.1002/cm.21174

Ebert B, Rautengarten C, McFarlane HE, Rupasinghe T, Zeng W, Ford K, Scheller HV, Bacic A, Roessner U, Persson S, et al. A Golgi UDP-GlcNAc transporter delivers substrates for N-linked glycans and sphingolipids. *Nat Plants*. 2018:4(10):792–801. https://doi.org/10.1038/s41477-018-0235-5

Engel BD, Schaffer M, Cuellar LK, Villa E, Plitzko JM, Baumeister W. Native architecture of the Chlamydomonas chloroplast revealed by in situ cryo-electron tomography. *eLife*. 2015:4:e04889. https://doi.org/10.7554/eLife.04889

Fahlgren N, Gehan MA, Baxter I. Lights, camera, action: high-throughput plant phenotyping is ready for a close-up. *Curr Opin Plant Biol*. 2015:24:93–99. https://doi.org/10.1016/j.pbi.2015.02.006

Fellers TJ, Davidson MW. Nikon microscopy U—coverslip correction; 2024 [accessed 2025 Jun 19]. https://www.microscopyu.com/microscopy-basics/coverslip-correction

Foster ED, Deardorff A. Open Science Framework (OSF). *J Med Library Assoc*. 2017:105(2):203–206. https://doi.org/10.5195/jmla.2017.88

Fujita M, Himmelspach R, Ward J, Whittington A, Hasenbein N, Liu C, Truong TT, Galway ME, Mansfield SD, Hocart CH, et al. The Anisotropy1 D604N mutation in the arabidopsis cellulose synthase1 catalytic domain reduces cell wall crystallinity and the velocity of cellulose synthase complexes. *Plant Physiol*. 2013:162(1):74–85. https://doi.org/10.1104/pp.112.211565

Galvan-Ampudia CS, Cerutti G, Legrand J, Brunoud G, Martin-Arevalillo R, Azais R, Bayle V, Moussu S, Wenzl C, Jaillais Y, et al. Temporal integration of auxin information for the regulation of patterning. *eLife*. 2020:9:e55832. https://doi.org/10.7554/eLife.55832

Gaudreault N. Illumination power, stability, and linearity measurements for confocal and widefield microscopes V2; 2022 [accessed 2025 Jun 19]. protocols.io. https://www.protocols.io/view/illumination-power-stability-and-linearity-measure-b68prhvn.

Geldner N, Dénervaud-Tendon V, Hyman DL, Mayer U, Stierhof Y-D, Chory J. Rapid, combinatorial analysis of membrane compartments in intact plants with a multicolor marker set. *Plant J*. 2009:59(1):169–178. https://doi.org/10.1111/j.1365-313X.2009.03851.x

Gilroy S. Fluorescence microscopy of living plant cells. *Annu Rev Plant Physiol Plant Mol Biol*. 1997:48(1):165–190. https://doi.org/10.1146/annurev.arplant.48.1.165

Gómez-Felipe A, Branchini E, Wang B, Marconi M, Bertrand-Rakusová H, Stan T, Burkiewicz J, de Folter S, Routier-Kierzkowska A-L, Wabnik K, et al. Two orthogonal differentiation gradients locally coordinate fruit morphogenesis. *Nat Commun*. 2024:15(1):2912. https://doi.org/10.1038/s41467-024-47325-1

Goodwin PC. Evaluating optical aberration using fluorescent microspheres: methods, analysis, and corrective actions. *Methods Cell Biol*. 2007:81:397–413. https://doi.org/10.1016/S0091-679X(06)81018-6

Grefen C, Blatt MR. A 2in1 cloning system enables Ratiometric Bimolecular Fluorescence Complementation (RBiFC). *BioTechniques*. 2012:53(5):311–314. https://doi.org/10.2144/000113941

Guerin CJ. Using antibodies in microscopy: a guide to immunohistochemistry. Part 1: antibodies, tissue fixation, embedding, and sectioning. *Microsc Today*. 2023a:31(2):26–31. https://doi.org/10.1093/mictod/qaad006

Guerin CJ. Using antibodies in microscopy: a guide to immunohistochemistry. Part 2: IHC staining protocols. *Microsc Today*. 2023b:31(3):34–39. https://doi.org/10.1093/mictod/qaad029

Halazonetis DJ. What do 8-bit and 12-bit grayscale mean and which should I use when scanning? *Am J Orthod Dentofac Orthop*. 2005:127(3):387–388. https://doi.org/10.1016/j.ajodo.2004.07.025

Hamant O, Heisler MG, Jönsson H, Krupinski P, Uyttewaal M, Bokov P, Corson F, Sahlin P, Boudaoud A, Meyerowitz EM, et al. Developmental patterning by mechanical signals in Arabidopsis. *Science*. 2008:322(5908):1650–1655. https://doi.org/10.1126/science.1165594

Hardham AR. Confocal microscopy in plant–pathogen interactions adrienne. In: Bolton MD, Thomma BPHJ, editors. *Plant fungal pathogens: methods and protocols, methods in molecular biology*. Vol. 835. Springer Science + Business Media; 2012. p. 295–309.

Hartley M, Kleywegt GJ, Patwardhan A, Sarkans U, Swedlow JR, Brazma A. The BioImage archive—building a home for life-sciences microscopy data. *J Mol Biol*. 2022:434(11):167505. https://doi.org/10.1016/j.jmb.2022.167505

Haseloff J. Imaging green fluorescent protein in transgenic plants. In: Rizzuto R, Fasolato C, editors. *Imaging living cells. Springer lab manual*. Berlin: Springer; 1999. p. 362–394. https://doi.org/10.1007/978-3-642-60003-6_16

Heddleston JM, Aaron JS, Khuon S, Chew T-L. A guide to accurate reporting in digital image acquisition—can anyone replicate your microscopy data? *J Cell Sci*. 2021:134(6):jcs254144. https://doi.org/10.1242/jcs.254144

Hepler PK, Gunning BES. Confocal fluorescence microscopy of plant cells. *Protoplasma*. 1998:201(3-4):121–157. https://doi.org/10.1007/BF01287411

Hériché M, Arnould C, Wipf D, Courty P-E. Imaging plant tissues: advances and promising clearing practices. *Trends Plant Sci*. 2022:27(6):601–615. https://doi.org/10.1016/j.tplants.2021.12.006

Herud-Sikimić O, Stiel AC, Kolb M, Shanmugaratnam S, Berendzen KW, Feldhaus C, Höcker B, Jürgens G. A biosensor for the direct visualization of auxin. *Nature*. 2021:592(7856):768–772. https://doi.org/10.1038/s41586-021-03425-2

Hervieux N, Dumond M, Sapala A, Routier-Kierzkowska A-L, Kierzkowski D, Roeder AHK, Smith RS, Boudaoud A, Hamant O. A mechanical feedback restricts sepal growth and shape in Arabidopsis. *Curr Biol*. 2016:26(8):1019–1028. https://doi.org/10.1016/j.cub.2016.03.004

Hickey SM, Ung B, Bader C, Brooks R, Lazniewska J, Johnson IRD, Sorvina A, Logan J, Martini C, Moore CR, et al. Fluorescence microscopy—an outline of hardware, biological handling, and fluorophore considerations. *Cells*. 2021:11(1):35. https://doi.org/10.3390/cells11010035

Hobson CM, Guo M, Vishwasrao HD, Wu Y, Shroff H, Chew T-L. Practical considerations for quantitative light sheet fluorescence microscopy. *Nat Methods*. 2022:19(12):1538–1549. https://doi.org/10.1038/s41592-022-01632-x

Hoffmann N, Mohammad E, McFarlane HE. Disrupting cell wall integrity impacts endomembrane trafficking to promote secretion over endocytic trafficking. *J Exp Bot*. 2024:75(12):3731–3747. https://doi.org/10.1093/jxb/erae195

Huynh J, Hotton SK, Chan R, Syed Y, Thomson J. Evaluation of novel surfactants for plant transformation. *BMC Res Notes*. 2022:15(1):360. https://doi.org/10.1186/s13104-022-06251-5

Iudin A, Korir PK, Salavert-Torres J, Kleywegt GJ, Patwardhan A. EMPIAR: a public archive for raw electron microscopy image data. *Nat Methods*. 2016:13(5):387–388. https://doi.org/10.1038/nmeth.3806

Iudin A, Korir PK, Somasundharam S, Weyand S, Cattavitello C, Fonseca N, Salih O, Kleywegt GJ, Patwardhan A. EMPIAR: the electron microscopy public image archive. *Nucleic Acids Res*. 2023:51(D1):D1503–D1511. https://doi.org/10.1093/nar/gkac1062

Jacques E, Verbelen J-P, Vissenberg K. Mechanical stress in Arabidopsis leaves orients microtubules in a 'continuous' supracellular pattern. *BMC Plant Biol*. 2013:13(1):163. https://doi.org/10.1186/1471-2229-13-163

Jambor H, Antonietti A, Alicea B, Audisio TL, Auer S, Bhardwaj V, Burgess SJ, Ferling I, Gazda MA, Hoeppner LH, et al. Creating clear and informative image-based figures for scientific publications. *PLoS Biol*. 2021:19(3):e3001161. https://doi.org/10.1371/journal.pbio.3001161

Jiang J. Fluorescence in situ hybridization in plants: recent developments and future applications. *Chromosome Res*. 2019:27(3):153–165. https://doi.org/10.1007/s10577-019-09607-z

Jones K, Kim DW, Park JS, Khang CH. Live-cell fluorescence imaging to investigate the dynamics of plant cell death during infection by the rice blast fungus *Magnaporthe oryzae*. *BMC Plant Biol*. 2016:16(1):69. https://doi.org/10.1186/s12870-016-0756-x

Jonkman J. Rigor and reproducibility in confocal fluorescence microscopy. *Cytometry Part A*. 2020:97(2):113–115. https://doi.org/10.1002/cyto.a.23924

Jonkman J, Brown CM, Wright GD, Anderson KI, North AJ. Guidance for quantitative confocal microscopy. *Nat Protoc*. 2020:15(5):1585–1611. https://doi.org/10.1038/s41596-020-0313-9

Jonkman J, Swoger J, Kress H, Rohrbach A, Stelzer EHK. [18] resolution in optical microscopy. In: Marriott G, Parker I, editors. *Methods in enzymology*. Academic Press; 2003. p. 416–446.

Jost AP-T, Waters JC. Designing a rigorous microscopy experiment: validating methods and avoiding bias. *J Cell Biol*. 2019:218(5):1452–1466. https://doi.org/10.1083/jcb.201812109

Kana R, Sediva B, Prasil O. Microdomains heterogeneity in the thylakoid membrane proteins visualized by super-resolution microscopy. *Photosynthetica*. 2023:61(SPECIAL ISSUE 2023-2):483–491. https://doi.org/10.32615/ps.2023.043

Kao P, Nodine MD. Application of expansion microscopy on developing Arabidopsis seeds. *Methods Cell Biol*. 2021:161:181–195. https://doi.org/10.1016/bs.mcb.2020.06.004

Keller HE. Objective lenses for confocal microscopy. In: *Handbook of biological confocal microscopy*. Powley JB, editor. Boston (MA): Springer US; 1990. p. 77–86.

Kirby AR, Gunning AP, Waldron KW, Morris VJ, Ng A. Visualization of plant cell walls by atomic force microscopy. *Biophys J*. 1996:70(3):1138–1143. https://doi.org/10.1016/S0006-3495(96)79708-4

Knapp E, Flores R, Scheiblin D, Modla S, Czymmek K, Yusibov V. A cryohistological protocol for preparation of large plant tissue sections for screening intracellular fluorescent protein expression. *BioTechniques*. 2012:52(1):31–37. https://doi.org/10.2144/000113778

Komis G, Šamajová O, Ovečka M, Šamaj J. Super-resolution microscopy in plant cell imaging. *Trends Plant Sci*. 2015:20(12):834–843. https://doi.org/10.1016/j.tplants.2015.08.013

Krebs M, Held K, Binder A, Hashimoto K, Den Herder G, Parniske M, Kudla J, Schumacher K. FRET-based genetically encoded sensors allow high-resolution live cell imaging of Ca 2+ dynamics. *Plant J*. 2012:69(1):181–192. https://doi.org/10.1111/j.1365-313X.2011.04780.x

Kurihara D, Mizuta Y, Sato Y, Higashiyama T. ClearSee: a rapid optical clearing reagent for whole-plant fluorescence imaging. *Development (Cambridge)*. 2015:142(23):4168–4179. https://doi.org/10.1242/dev.127613

Lambert TJ. FPbase: a community-editable fluorescent protein database. *Nat Methods*. 2019:16(4):277–278. https://doi.org/10.1038/s41592-019-0352-8

Lathe RS, McFarlane HE, Kesten C, Wang L, Khan GA, Ebert B, Ramírez-Rodríguez EA, Zheng S, Noord N, Frandsen K, et al. NKS1/ELMO4 is an integral protein of a pectin synthesis protein complex and maintains Golgi morphology and cell adhesion in Arabidopsis. *Proc Natl Acad Sci U S A*. 2024:121(15):e2321759121. https://doi.org/10.1073/pnas.2321759121

Le Gloanec C, Gómez-Felipe A, Alimchandani V, Branchini E, Bauer A, Routier-Kierzkowska A-L, Kierzkowski D. Modulation of cell differentiation and growth underlies the shift from bud protection to light capture in cauline leaves. *Plant Physiol*. 2024:196(2):1214–1230. https://doi.org/10.1093/plphys/kiae408

Lee J-Y, Kitaoka M. A beginner's guide to rigor and reproducibility in fluorescence imaging experiments. *Mol Biol Cell*. 2018:29(13):1519–1525. https://doi.org/10.1091/mbc.E17-05-0276

Lee KJD, Knox JP. Resin embedding, sectioning, and immunocytochemical analyses of plant cell walls in hard tissues. *Methods Mol Biol*. 2014:1080:41–52. https://doi.org/10.1007/978-1-62703-643-6_3

Lee RM, Eisenman LR, Khuon S, Aaron JS, Chew T-L. Believing is seeing—the deceptive influence of bias in quantitative microscopy. *J Cell Sci*. 2024:137(1):jcs261567. https://doi.org/10.1242/jcs.261567

Leroux O. Vibratome sectioning of plant materials for (immuno)cytochemical staining. In: Popper Z, editor. *The plant cell wall. Methods in molecular biology*. New York (NY): Humana Press; 2020. p. 339–350.

Leung BO, Chou KC. Review of super-resolution fluorescence microscopy for biology. *Appl Spectrosc*. 2011:65(9):967–980. https://doi.org/10.1366/11-06398

Lichtman JW, Conchello J-A. Fluorescence microscopy. *Nat Methods*. 2005:2(12):910–919. https://doi.org/10.1038/nmeth817

Lindeboom JJ, Nakamura M, Hibbel A, Shundyak K, Gutierrez R, Ketelaar T, Emons AMC, Mulder BM, Kirik V, Ehrhardt DW. A mechanism for reorientation of cortical microtubule arrays driven by microtubule severing. *Science*. 2013:342(6163):1245533. https://doi.org/10.1126/science.1245533

Lipsitch M, Tchetgen ET, Cohen T. Negative controls: a tool for detecting confounding and bias in observational studies. *Epidemiology*. 2010:21(3):383–388. https://doi.org/10.1097/EDE.0b013e3181d61eeb

Lisenbee CS, Karnik SK, Trelease RN. Overexpression and mislocalization of a tail-anchored GFP redefines the identity of peroxisomal ER. *Traffic*. 2003:4(7):491–501. https://doi.org/10.1034/j.1600-0854.2003.00107.x

Littlejohn GR, Gouveia JD, Edner C, Smirnoff N, Love J. Perfluorodecalin enhances in vivo confocal microscopy resolution of *Arabidopsis thaliana* mesophyll. *New Phytolog*. 2010:186(4):1018–1025. https://doi.org/10.1111/j.1469-8137.2010.03244.x

Littlejohn GR, Mansfield JC, Christmas JT, Witterick E, Fricker MD, Grant MR, Smirnoff N, Everson RM, Moger J, Love J. An update: improvements in imaging perfluorocarbon-mounted plant leaves with implications for studies of plant pathology, physiology, development and cell biology. *Front Plant Sci*. 2014:5:140. https://doi.org/10.3389/fpls.2014.00140

Lord SJ, Velle KB, Mullins RD, Fritz-Laylin LK. SuperPlots: communicating reproducibility and variability in cell biology. *J Cell Biol*. 2020:219(6):e202001064. https://doi.org/10.1083/jcb.202001064

Mahmoudian J, Hadavi R, Jeddi-Tehrani M, Mahmoudi AR, Bayat AA, Shaban E, Vafakhah M, Darzi M, Tarahomi M, Ghods R. Comparison of the photobleaching and photostability traits of Alexa Fluor 568- and fluorescein isothiocyanate- conjugated antibody. *Cell J*. 2011:13(3):169–172. PMCID: PMC3584473. https://pubmed.ncbi.nlm.nih.gov/23508937/

Malabadi RB, Teixeira Da Silva JA, Nataraja K. Green fluorescent protein in the genetic transformation of plants. *Transgenic Plant J*. 2008:2(2):86–109.

Marion J, Le Bars R, Satiat-Jeunemaitre B, Boulogne C. Optimizing CLEM protocols for plants cells: GMA embedding and cryosections as alternatives for preservation of GFP fluorescence in Arabidopsis roots. *J Struct Biol*. 2017:198(3):196–202. https://doi.org/10.1016/j.jsb.2017.03.008

Marqués G, Pengo T, Sanders MA. Imaging methods are vastly underreported in biomedical research. *eLife*. 2020:9:e55133. https://doi.org/10.7554/eLife.55133

Marques P, Strong J, Strader T, Hsia R. Optimization of automated immuno EM for both pre- and post-embedding labeling. *Microsc Microanal*. 2018:24(S1):1300–1301. https://doi.org/10.1017/S1431927618006980

Martin C, Blatt M. Manipulation and misconduct in the handling of image data. *Plant Cell*. 2013:25(9):3147–3148. https://doi.org/10.1105/tpc.113.250980

McNally JG, Karpova T, Cooper J, Conchello JA. Three-dimensional imaging by deconvolution microscopy. *Methods*. 1999:19(3):373–385. https://doi.org/10.1006/meth.1999.0873

McNamara G. Fluorophores-Table; 2024 [accessed 2025 Jun 19]. https://www.geomcnamara.com/fluorophore-table

Mizuta Y. Advances in two-photon imaging in plants. *Plant Cell Physiol*. 2021:62(8):1224–1230. https://doi.org/10.1093/pcp/pcab062

Monshausen GB, Messerli MA, Gilroy S. Imaging of the Yellow Cameleon 3.6 indicator reveals that elevations in cytosolic Ca2+ follow oscillating increases in growth in root hairs of Arabidopsis. *Plant Physiol*. 2008:147(4):1690–1698. https://doi.org/10.1104/pp.108.123638

Montero Llopis P, Senft RA, Ross-Elliott TJ, Stephansky R, Keeley DP, Koshar P, Marqués G, Gao Y-S, Carlson BR, Pengo T, et al. Best practices and tools for reporting reproducible fluorescence microscopy methods. *Nat Methods*. 2021:18(12):1463–1476. https://doi.org/10.1038/s41592-021-01156-w

Moore I, Murphy A. Validating the location of fluorescent protein fusions in the endomembrane system. *Plant Cell*. 2009:21(6):1632–1636. https://doi.org/10.1105/tpc.109.068668

Munafò MR, Nosek BA, Bishop DVM, Button KS, Chambers CD, du Sert NP, Simonsohn U, Wagenmakers E-J, Ware JJ, Ioannidis JPA. A manifesto for reproducible science. *Nat Hum Behav*. 2017:1(1):0021. https://doi.org/10.1038/s41562-016-0021

Nebenführ A, Gallagher LA, Dunahay TG, Frohlick JA, Mazurkiewicz AM, Meehl JB, Staehelin LA. Stop-and-go movements of plant Golgi stacks are mediated by the acto-myosin system. *Plant Physiol*. 1999:121(4):1127–1141. https://doi.org/10.1104/pp.121.4.1127

Nelson BK, Cai X, Nebenführ A. A multicolored set of in vivo organelle markers for co-localization studies in Arabidopsis and other plants. *Plant J*. 2007:51(6):1126–1136. https://doi.org/10.1111/j.1365-313X.2007.03212.x

Nelson G, Alexopoulos I, Azevedo M, Barachati F, Belyaev Y, Carvalho MT, Cesbron Y, Dauphin A, Corbett AD, Gelman L, et al. Monitoring the point spread function for quality control of confocal microscopes. 2022. https://doi.org/10.17504/protocols.io.bp2l61ww1vqe/v1

Noble E, Kumar S, Görlitz FG, Stain C, Dunsby C, French PMW. In vivo label-free mapping of the effect of a photosystem II inhibiting herbicide in plants using chlorophyll fluorescence lifetime. *Plant Methods*. 2017:13(1):48. https://doi.org/10.1186/s13007-017-0201-7

North AJ. Seeing is believing? A beginners' guide to practical pitfalls in image acquisition. *J Cell Biol*. 2006:172(1):9–18. https://doi.org/10.1083/jcb.200507103

Nybo K. GFP imaging in fixed cells. *BioTechniques*. 2012:52(6):359–360. https://doi.org/10.2144/000113872

Ono M, Murakami T, Kudo A, Isshiki M, Sawada H, Segawa A. Quantitative comparison of anti-fading mounting media for confocal laser scanning microscopy. *J Histochem Cytochem*. 2001:49(3):305–311. https://doi.org/10.1177/002215540104900304

Oreopoulos J, Berman R, Browne M. Spinning-disk confocal microscopy. *Methods Cell Biol*. 2014:123(123):153–175. https://doi.org/10.1016/B978-0-12-420138-5.00009-4

Otegui MS, Pennington JG. Electron tomography in plant cell biology. *Microscopy*. 2019:68(1):69–79. https://doi.org/10.1093/jmicro/dfy133

Ovečka M, Sojka J, Tichá M, Komis G, Basheer J, Marchetti C, Šamajová O, Kuběnová L, Šamaj J. Imaging plant cells and organs with light-sheet and super-resolution microscopy. *Plant Physiol*. 2022:188(2):683–702. https://doi.org/10.1093/plphys/kiab349

Ovečka M, von Wangenheim D, Tomančák P, Šamajová O, Komis G, Šamaj J. Multiscale imaging of plant development by light-sheet fluorescence microscopy. *Nat Plants*. 2018:4(9):639–650. https://doi.org/10.1038/s41477-018-0238-2

Pawley JB. ed. Points, pixels, and gray levels: digitizing image data. In: *Handbook of biological confocal microscopy*. Boston (MA): Springer US; 2006. p. 59–79.

Pawley J. The 39 steps: a cautionary tale of quantitative 3-D fluorescence microscopy. *BioTechniques*. 2000:28(5):884–887. https://doi.org/10.2144/00285bt01

Piccinini L, Ramamonjy FN, Ursache R. Imaging plant cell walls using fluorescent stains: the beauty is in the details. *J Microsc*. 2024:295(2):102–120. https://doi.org/10.1111/jmi.13289

Piña R, Santos-Díaz AI, Orta-Salazar E, Aguilar-Vazquez AR, Mantellero CA, Acosta-Galeana I, Estrada-Mondragon A, Prior-Gonzalez M, Martinez-Cruz JI, Rosas-Arellano A. Ten approaches that improve immunostaining: a review of the latest advances for the optimization of immunofluorescence. *Int J Mol Sci*. 2022:23(3):1426. https://doi.org/10.3390/ijms23031426

Piovesan A, Vancauwenberghe V, Van De Looverbosch T, Verboven P, Nicolaï B. X-ray computed tomography for 3D plant imaging. *Trends Plant Sci*. 2021:26(11):1171–1185. https://doi.org/10.1016/j.tplants.2021.07.010

Prieto P, Moore G, Shaw P. Fluorescence in situ hybridization on vibratome sections of plant tissues. *Nat Protoc*. 2007:2(7):1831–1838. https://doi.org/10.1038/nprot.2007.265

Prunet N, Jack TP, Meyerowitz EM. Live confocal imaging of Arabidopsis flower buds. *Dev Biol*. 2016:419(1):114–120. https://doi.org/10.1016/j.ydbio.2016.03.018

Russ JC. Chapter 5. Image enhancement (processing in the spatial domain). In: Russ JC, editor. *The image processing handbook*. Boca Raton: CRC Press; 2006. p. 269–328.

Sakamoto Y, Ishimoto A, Sakai Y, Sato M, Nishihama R, Abe K, Sano Y, Furuichi T, Tsuji H, Kohchi T, et al. Improved clearing method contributes to deep imaging of plant organs. *Commun Biol*. 2022:5(1):12. https://doi.org/10.1038/s42003-021-02955-9

Samalova M, Fricker M, Moore I. Ratiometric fluorescence-imaging assays of plant membrane traffic using polyproteins. *Traffic*. 2006:7(12):1701–1723. https://doi.org/10.1111/j.1600-0854.2006.00502.x

Sawchuk MG, Head P, Donner TJ, Scarpella E. Time-lapse imaging of Arabidopsis leaf development shows dynamic patterns of procambium formation. *New Phytolog*. 2007:176(3):560–571. https://doi.org/10.1111/j.1469-8137.2007.02193.x

Scheuring D, Minina EA, Krueger F, Lupanga U, Krebs M, Schumacher K. Light at the end of the tunnel: FRAP assays combined with super resolution microscopy confirm the presence of a tubular vacuole network in meristematic plant cells. *Plant Cell*. 2024:36(11):4683–4691. https://doi.org/10.1093/plcell/koae243

Schindelin J, Arganda-Carreras I, Frise E, Kaynig V, Longair M, Pietzsch T, Preibisch S, Rueden C, Saalfeld S, Schmid B, et al. Fiji: an open-source platform for biological-image analysis. *Nat Methods*. 2012:9(7):676–682. https://doi.org/10.1038/nmeth.2019

Schmied C, Nelson MS, Avilov S, Bakker G-J, Bertocchi C, Bischof J, Boehm U, Brocher J, Carvalho MT, Chiritescu C, et al. Community-developed checklists for publishing images and image analyses. *Nat Methods*. 2024:21(2):170–181. https://doi.org/10.1038/s41592-023-01987-9

Schneider R, Ehrhardt DW, Meyerowitz EM, Sampathkumar A. Tethering of cellulose synthase to microtubules dampens mechano-induced cytoskeletal organization in Arabidopsis pavement cells. *Nat Plants*. 2022:8(9):1064–1073. https://doi.org/10.1038/s41477-022-01218-7

Schubert V. Super-resolution microscopy—applications in plant cell research. *Front Plant Sci*. 2017:8:531. https://doi.org/10.3389/fpls.2017.00531

Scipioni L, Lanzanó L, Diaspro A, Gratton E. Comprehensive correlation analysis for super-resolution dynamic fingerprinting of cellular compartments using the Zeiss Airyscan detector. *Nat Commun*. 2018:9(1):5120. https://doi.org/10.1038/s41467-018-07513-2

Segami S, Makino S, Miyake A, Asaoka M, Maeshima M. Dynamics of vacuoles and H+-pyrophosphatase visualized by monomeric green fluorescent protein in Arabidopsis: artifactual bulbs and native intravacuolar spherical structures. *Plant Cell*. 2014:26(8):3416–3434. https://doi.org/10.1105/tpc.114.127571

Shaner NC, Lambert GG, Chammas A, Ni Y, Cranfill PJ, Baird MA, Sell BR, Allen JR, Day RN, Israelsson M, et al. A bright monomeric green fluorescent protein derived from *Branchiostoma lanceolatum*. *Nat Methods*. 2013:10(5):407–409. https://doi.org/10.1038/nmeth.2413

Shaw SL, Ehrhardt DW. Smaller, faster, brighter: advances in optical imaging of living plant cells. *Annu Rev Plant Biol*. 2013:64(1):351–375. https://doi.org/10.1146/annurev-arplant-042110-103843

Shimamura, M. Whole-mount immunofluorescence staining of plant cells and tissues. In: *Plant microtechniques and protocols*. Yeung ECT, Stasolla C, Sumner MJ and Huang BQ eds, Cham: Springer International Publishing; 2015. p. 181–196.

Sicilia M-A, García-Barriocanal E, Sánchez-Alonso S. Community curation in open dataset repositories: insights from Zenodo. *Proc Comput Sci*. 2017:106:54–60. https://doi.org/10.1016/j.procs.2017.03.009

Silveira SR, Le Gloanec C, Gómez-Felipe A, Routier-Kierzkowska A-L, Kierzkowski D. Live-imaging provides an atlas of cellular growth dynamics in the Stamen. *Plant Physiol*. 2022:188(2):769–781. https://doi.org/10.1093/plphys/kiab363

Spring KR. Detectors for fluorescence microscopy. In: *Methods in cellular imaging*. Periasamy A ed. New York (NY): Springer; 2001. p. 40–52.

Staudt T, Hell SW. Adaptive correction technique for 3D reconstruction of fluorescence microscopy images. *Microsc Res Tech*. 2008:71(2):146–157. https://doi.org/10.1002/jemt.20536

Stewart CN Jr. The utility of green fluorescent protein in transgenic plants. *Plant Cell Rep*. 2001:20(5):376–382. https://doi.org/10.1007/s002990100346

Stirling DR, Swain-Bowden MJ, Lucas AM, Carpenter AE, Cimini BA, Goodman A. CellProfiler 4: improvements in speed, utility and usability. *BMC Bioinformatics*. 2021:22(1):433. https://doi.org/10.1186/s12859-021-04344-9

Strauss S, Runions A, Lane B, Eschweiler D, Bajpai N, Trozzi N, Routier-Kierzkowska A-L, Yoshida S, da Silveira SR, Vijayan A, et al. Using positional information to provide context for biological image analysis with MorphoGraphX 2.0. *eLife*. 2022:11:e72601. https://doi.org/10.7554/eLife.72601

Swedlow JR. Quantitative fluorescence microscopy and image deconvolution. *Methods Cell Biol*. 2007:81:447–465. https://doi.org/10.1016/S0091-679X(06)81021-6

Sydor AM, Czymmek KJ, Puchner EM, Mennella V. Super-resolution microscopy: from single molecules to supramolecular assemblies. *Trends Cell Biol*. 2015:25(12):730–748. https://doi.org/10.1016/j.tcb.2015.10.004

Tanz SK, Castleden I, Small ID, Millar AH. Fluorescent protein tagging as a tool to define the subcellular distribution of proteins in plants. *Front Plant Sci*. 2013:4:214. https://doi.org/10.3389/fpls.2013.00214

Thermofisher. Thermofisher Fluorescence SpectraViewer; 2024 [accessed 2025 Jun 19]. https://www.thermofisher.com/order/fluorescence-spectraviewer/#!/

Tirichine L, Andrey P, Biot E, Maurin Y, Gaudin V. 3D fluorescent in situ hybridization using Arabidopsis leaf cryosections and isolated nuclei. *Plant Methods*. 2009:5(1):11. https://doi.org/10.1186/1746-4811-5-11

Torday JS, Baluška F. Why control an experiment? *EMBO Rep*. 2019:20(10):e49110. https://doi.org/10.15252/embr.201949110

Truernit E, Bauby H, Dubreucq B, Grandjean O, Runions J, Barthélémy J, Palauqui J-C. High-resolution whole-mount imaging of three-dimensional tissue organization and gene expression enables the study of phloem development and structure in Arabidopsis. *Plant Cell*. 2008:20(6):1494–1503. https://doi.org/10.1105/tpc.107.056069

Truernit E, Haseloff J. A simple way to identify non-viable cells within living plant tissue using confocal microscopy. *Plant Methods*. 2008:4(1):15. https://doi.org/10.1186/1746-4811-4-15

Ueda H, Yokota E, Kutsuna N, Shimada T, Tamura K, Shimmen T, Hasezawa S, Dolja VV, Hara-Nishimura I. Myosin-dependent endoplasmic reticulum motility and F-actin organization in plant cells. *Proc Natl Acad Sci U S A*. 2010:107(15):6894–6899. https://doi.org/10.1073/pnas.0911482107

Verbančič J, Huang JJ, McFarlane HE. Analysis of cellulose synthase activity in arabidopsis using spinning disk microscopy. *STAR Protoc*. 2021:2(4):100863. https://doi.org/10.1016/j.xpro.2021.100863

von Wangenheim D, Hauschild R, Fendrych M, Barone V, Benková E, Friml J. Live tracking of moving samples in confocal microscopy for vertically grown roots. *eLife*. 2017:6:e26792. https://doi.org/10.7554/eLife.26792

Voss U, Larrieu A, Wells DM. From Jellyfish to biosensors: the use of fluorescent proteins in plants. *Int J Dev Biol*. 2013:57(6-7-8):525–533. https://doi.org/10.1387/ijdb.130208dw

Waadt R, Kudla J. In planta visualization of protein interactions using Bimolecular Fluorescence Complementation (BiFC). *Cold Spring Harb Protoc*. 2008:2008(4):pdb.prot4995. https://doi.org/10.1101/pdb.prot4995

Wan Y, Ash WM, Fan L, Hao H, Kim MK, Lin J. Variable-angle total internal reflection fluorescence microscopy of intact cells of *Arabidopsis thaliana*. *Plant Methods*. 2011:7(1):27. https://doi.org/10.1186/1746-4811-7-27

Wang B, Bauer A, Gómez-Felipe A, Silveira S, Kierzkowski D. Confocal live imaging of reproductive organs development in Arabidopsis. *Bio Protoc*. 2025:15:1364. https://doi.org/10.21769/BioProtoc.5177

Wang H, Fu T, Du Y, Gao W, Huang K, Liu Z, Chandak P, Liu S, Van Katwyk P, Deac A, et al. Scientific discovery in the age of artificial intelligence. *Nature*. 2023:620(7972):47–60. https://doi.org/10.1038/s41586-023-06221-2

Wang J, Mylle E, Johnson A, Besbrugge N, De Jaeger G, Friml J, Pleskot R, Van Damme D. High temporal resolution reveals simultaneous plasma membrane recruitment of TPLATE complex subunits. *Plant Physiol*. 2020:183(3):986–997. https://doi.org/10.1104/pp.20.00178

Wang Y-S, Yoo C-M, Blancaflor EB. Improved imaging of actin filaments in transgenic Arabidopsis plants expressing a green fluorescent protein fusion to the C- and N-termini of the fimbrin actin-binding domain 2. *New Phytol*. 2008:177(2):525–536. https://doi.org/10.1111/j.1469-8137.2007.02261.x

Waters JC. Accuracy and precision in quantitative fluorescence microscopy. *J Cell Biol*. 2009:185(7):1135–1148. https://doi.org/10.1083/jcb.200903097

Wernersson E, Gelali E, Girelli G, Wang S, Castillo D, Langseth CM, Verron Q, Nguyen HQ, Chattoraj S, Casals AM, et al. Deconwolf enables high-performance deconvolution of widefield fluorescence microscopy images. *Nat Methods*. 2024:21(7):1245–1256. https://doi.org/10.1038/s41592-024-02294-7

Westbrook JD, Young JY, Shao C, Feng Z, Guranovic V, Lawson CL, Vallat B, Adams PD, Berrisford JM, Bricogne G, et al. PDBx/MmCIF ecosystem: foundational semantic tools for structural biology. *J Mol Biol*. 2022:434(11):167599. https://doi.org/10.1016/j.jmb.2022.167599

Wickramanayake JS, Czymmek KJ. A conventional fixation volume electron microscopy protocol for plants. *Methods Cell Biol*. 2023:177:83–99. https://doi.org/10.1016/bs.mcb.2023.04.008

Wightman R. An overview of cryo-scanning electron microscopy techniques for plant imaging. *Plants*. 2022:11(9):1113. https://doi.org/10.3390/plants11091113

Wilkinson MD, Dumontier M, Aalbersberg IJJ, Appleton G, Axton M, Baak A, Blomberg N, Boiten J-W, da Silva Santos LB, Bourne PE, et al. The FAIR guiding principles for scientific data management and stewardship. *Sci Data*. 2016:3(1):160018. https://doi.org/10.1038/sdata.2016.18

Wilson SM, Bacic A. Preparation of plant cells for transmission electron microscopy to optimize immunogold labeling of carbohydrate and protein epitopes. *Nat Protoc*. 2012:7(9):1716–1727. https://doi.org/10.1038/nprot.2012.096

Wu Q, Luo A, Zadrozny T, Sylvester A, Jackson D. Fluorescent protein marker lines in maize: generation and applications. *Int J Dev Biol*. 2013:57(6-7-8):535–543. https://doi.org/10.1387/ijdb.130240qw

Yoshida SR, Maity BK, Chong S. Visualizing protein localizations in fixed cells: caveats and the underlying mechanisms. *J Phys Chem B*. 2023:127(19):4165–4173. https://doi.org/10.1021/acs.jpcb.3c01658

Yu HY, Seo JA, Kim JE, Han KH, Shim WB, Yun SH, Lee YW. Functional analyses of heterotrimeric G protein gα and gβ subunits in *Gibberella zeae*. *Microbiology*. 2008:154(2):392–401. https://doi.org/10.1099/mic.0.2007/012260-0

Zhao H, Tan Z, Wen X, Wang Y. An improved syringe agroinfiltration protocol to enhance transformation efficiency by combinative use of 5-azacytidine, ascorbate acid and Tween-20. *Plants*. 2017:6(1):9. https://doi.org/10.3390/plants6010009

Zhou R, Liu H, Ju T, Dixit R. Quantifying the polymerization dynamics of plant cortical microtubules using kymograph analysis. *Methods Cell Biol*. 2020:160(160):281–293. https://doi.org/10.1016/bs.mcb.2020.04.006

Zhu M, Chen W, Mirabet V, Hong L, Bovio S, Strauss S, Schwarz EM, Tsugawa S, Wang Z, Smith RS, et al. Robust organ size requires robust timing of initiation orchestrated by focused auxin and cytokinin signalling. *Nat Plants*. 2020:6(6):686–698. https://doi.org/10.1038/s41477-020-0666-7

Zimmermann T, Marrison J, Hogg K, O'Toole P. Clearing up the signal: spectral imaging and linear unmixing in fluorescence microscopy. In: Paddock S, editor. *Confocal microscopy*. New York(NY): Humana Press; 2014. p. 129–148.

Zou Y, Tang W, Li B. Exploring natural product biosynthesis in plants with mass spectrometry imaging. *Trends Plant Sci*. 2025:30(1):69–84. https://doi.org/10.1016/j.tplants.2024.08.002